Nat. Hazards Earth Syst. Sci. Discuss., https://doi.org/10.5194/nhess-2018-148
Manuscript under review for journal Nat. Hazards Earth Syst. Sci.
Discussion started: 10 July 2018

Natural Hazards and Earth System Sciences
Open Access
EGU
Discussions

Estimation of path attenuation and site characteristics in the north-west Himalaya and its adjoining area using generalized inversion method

Harinarayan, Nelliparambil Hareeshkumar[1], Abhishek Kumar[*2]

[1, 2] Department of Civil Engineering, Indian Institute of Technology Guwahati, Assam, India.

Corresponding to: Kumar Abhishek (abhitoaashu@gmail.com/ abhiak@iitg.ernet.in)

Abstract. Present work focuses on the determination of path attenuation as well as site characteristics of PESMOS managed recording stations, located in the north-west Himalaya and its adjoining region, using two-step generalized inversion technique. In the first step of inversion, non-parametric attenuation curves are developed. Presence of a kink is observed at around 105km hypocentral distance while correlating the path attenuation with the hypocentral distance indicating the presence of Moho discontinuity in the region. Further, $Q_s = 105\, f^{0.94}$ as S wave quality factor within 105km, is obtained indicating that the region is possibly heterogeneous as well as seismically active. In the second step of inversion, site amplification curves are developed separately from the attenuation corrected data for horizontal and vertical components of the accelerogram. Further, site amplification spectra is computed as the ratio of the obtained horizontal and vertical components to determine the amplification function and predominant frequency for each of the PESMOS managed recording stations, exist within the study area. The predominant frequency estimated by generalized inversion method are in good agreement with those obtained using horizontal to vertical spectral ratio of the S wave portion of the accelerogram. Maps showing spatial distribution of predominant frequencies and amplification functions across the study region are also developed based on the present work.

Keywords: *PESMOS recording stations, Northwest Himalaya, path attenuation, site characteristics, Generalized Inversion, HVSR*

Nat. Hazards Earth Syst. Sci. Discuss., https://doi.org/10.5194/nhess-2018-148
Manuscript under review for journal Nat. Hazards Earth Syst. Sci.
Discussion started: 10 July 2018

1 Introduction

The Himalayan arc extends approximately 2500km starting from Kashmir in the northwest to Arunachal Pradesh in the northeast and is considered as one of the most seismically active regions in the world. This region has experienced several destructive earthquakes (EQs) including 4 great EQs (1897 Shillong EQ, 1905 Kangra EQ, 1950 Assam EQ and 1934 Bihar-Nepal EQ) in the last 120 years. Based on the seismic activity, the entire Himalayan belt can be subdivided into three distinct segments namely the western, the central and the eastern segments (Philip, 2014). The region of the north-west Himalaya and its foothills within India encompassing the states of Punjab, Uttarakhand, Delhi, Haryana and Himachal Pradesh come under seismic zone IV and V as per IS 1893: 2002 indicating high to very high seismicity. Therefore, the necessity of precise seismic hazard studies of this region has become an issue of great importance.

The intensity of ground shaking during an EQ at a particular site is a function of source, path and site parameters. Source parameters includes magnitude, fault mechanism, stress drop and rupture process. On the other hand, path parameters include geometric attenuation and loss of seismic energy due to the anelasticity of the earth and scattering of elastic waves in heterogeneous media. Similarly, site characteristics include modification of amplitude, frequency content and duration of the incoming seismic wave by subsurface medium as reached to the surface. Determinations of aforementioned EQ parameters are important for development of region specific GMPES which can be used for region/ site specific seismic hazard assessment. Above parameters are commonly estimated using EQ records and some spectral modelling or inversion approach like generalized inversion method (Andrews 1986; Castro et al., 1990; Oth et al., 2009 etc.).

In the present study, EQ records from the region of the north-west Himalaya and its foothills, obtained from PESMOS database are analysed for estimating path attenuation and site characteristics separately, using a two-step generalized inversion of the S-wave amplitude spectra (hereafter referred to as GINV). In the first step, attenuation curves are developed using a non-parametric inversion approach similar to Castro et al., (1990) and Oth et al., (2008). In the conventional generalized inversion method (Andrews, 1986; Hartzell, 1992), site and source terms are estimated simultaneously in the second step of inversion, by inverting the S-wave (or Coda wave) spectra corrected for the path parameter. This method requires a reference site (whose site amplification is known) in-order to remove the trade-off between the source and site parameters (Andrews 1986). In case of PESMOS database, however, due to the lack of detailed knowledge about the geology beneath the recording stations, identifying a reference site is not possible. In the absence of a reference site, only the site parameter is evaluated in the second step of inversion, using a non-reference generalized inversion approach (similar to the work by Joshi et al., 2010; Harinarayan and Kumar 2017). The obtained site terms are compared with the horizontal and vertical ratios (HVSR) calculated from the same S-wave window as used in the GINV above.

This study is one of the first attempts in the area to systematically evaluate path and site parameters using a larger database. Available sudies on attenuation characteristics of north-west Himalaya are in fact based on considering few EQ records from limited recording stations. These include; Joshi (2006) estimated frequency independent S wave quality factor (Q_s) for the Garhwal Himalayas using 1991 Uttarkashi EQ and 1999 Chamoli EQ ground motions from 8 recording stations. In another study, Singh et al., (2012) estimated frequency depended Q_s for the Kumaun Himalays using 23 EQ events, from 9 recording stations applying the extended coda-normalization method. Similarly, Negi et al., (2015) and Tripathi et al., (2015) estimated Q_s for the

Nat. Hazards Earth Syst. Sci. Discuss., https://doi.org/10.5194/nhess-2018-148
Manuscript under review for journal Nat. Hazards Earth Syst. Sci.
Discussion started: 10 July 2018

Natural Hazards and Earth System Sciences
Open Access
Discussions

Garhwal Himalayas. The aforementioned studies did not highlight the attenuation characteristics of the entire north-west Himalaya region. In addition, similar to path attenuation studies, very few literatures on the determination of site characteristics from EQ records have been reported for this region. These include work Nath et al., (2002) which computed site terms using the aftershocks of the 1999 Chamoli EQ from 5 recording stations located in the Uttarakhand region. Similarly, by Sharma et al., (2014) using EQ records in context of generalized inversion and horizontal to vertical spectral ratio to estimate site parameters for the Garhwal region of Uttarakhand. In another work, Harinarayan and Kumar (2017) reported a comparative study on site characteristics computed using EQ records from Tarai region of Uttarakhand using multiple analytical approaches. In another recent work, Harinarayan and Kumar (2018) computed site parameters in terms of predominant frequency (f_{peak}) alone, utilizing the EQ records from the north-west Himalaya and nearby regions using spectral ratio method. Site characteristics in terms of amplification function (A_{peak}) for the recording stations have been missed in Harinarayan and Kumar (2018). In the present study, site characteristics are determined in terms of f_{peak} and A_{peak}. Further, maps showing spatial distribution of f_{peak} and A_{peak} are separately developed for regions of Delhi, Uttarakhand, Punjab and Himachal Pradesh in this work. Such maps can be of utmost importance for seismic site classification, ground response analyses and microzonation studies in the future works.

2 Database

The input data used in this study consists of three components accelerograms obtained from PESMOS database available at http://www.pesmos.in/. The instrumentation used for recording EQs consists of internal AC-63 GeoSIG triaxial force balanced accelerometers and GSR-18 GeoSIG 18 bit digitizers with external GPS (Kumar et al. 2012). Ground motion recordings are done in trigger mode during each EQ with a sampling rate of 200 per second.

In the present analysis, ground motions records corresponding to EQs happened between 2004 and 2017 are used. For estimating site characteristics, 341 records from 86 EQs, with magnitudes ranging from Mw=2.3 to Mw=5.8, having focal depths ranging from 2 to 80km are used. Further, these records are corresponding to 101 recording stations, located in the hypocentral distance ranging from 10 to 85km. Coordinates of each of the recording station, used in this work are listed in Table 1, columns 2 and 3. Further, details of EQs used for estimating site characteristics are summarized in Table 2.

For estimating path attenuation however, only those EQs, which are recorded at atleast two recording stations in which at least one recording station should be located within hypocentral distance equal to or less than the reference distance (reference distance is discussed under section 'Spectral attenuation with distance) are considered. Thus, not all recording stations whose records are used for computing site characteristics satisfy the above reference distance criteria, are considered in path attenuation determination. Out of 341 EQ records used for estimating site parameters, only 207 EQ records satisfies the reference distance criteria. Satisfying the reference distance criteria, the database for estimating path attenuation consists of 207 records from 32 EQs, with magnitude ranging from Mw= 3.1 to Mw=5.5, with focal depths ranging from 3 to 20km, recorded at 69 recording stations and within hypocentral distance ranging from 9 to 200km. Table 3 summarizes the details of

Nat. Hazards Earth Syst. Sci. Discuss., https://doi.org/10.5194/nhess-2018-148
Manuscript under review for journal Nat. Hazards Earth Syst. Sci.
Discussion started: 10 July 2018

the dataset used for estimating path attenuation. In addition, Figure 1 shows the source-to-recording station path coverage of all the data set used in the present study.

2.1 Data processing

All the EQ records collected above, are corrected for baseline correction following a 5% cosine taper and a band-pass filtering, between the frequency range of 0.25Hz and 20Hz, using a Butterworth filter. Further, time windows starting about 0.5s before the onset of the S wave and ending when 90% of the total seismic energy of the EQ record is reached, are separated and tapered with a 5% cosine window (Ameri et al., 2011; Bindi et al., 2009). Typical lengths of the time windows for the present analysis vary from 4 to 15s. Further, for some of the records, where the window length obtained is longer than 15s, it is fixed to 15s in order to avoid a record having too much of coda wave energy in the analysis time window (Oth et al., 2008). Later, based on the extracted windows, the Fourier amplitude spectra is calculated for each EQ record, smoothened by applying the Konno and Ohmachi (1999) algorithm, with the smoothing parameter "b" = 20.

For further analysis, path and site parameters are estimated using two separate inversion procedures using earlier discussed EQ database, as discussed separately in the following sections.

3 Path attenuation

In the first step of inversion, spectral path attenuation curves are developed by eliminating the effect of site parameter, thereby retaining only the source and path attenuation characteristics. All EQ records, irrespective of whether located on soil or rock site can be utilized for inversion. Thus, present method is very much suitable for PESMOS database where accurate site characteristics of recording stations are not available. The horizontal portion of the accelerograms, obtained by the root mean square average of the east-west and north-south components is considered for developing path attenuation curves. Detailed discussions on the method can be found in following sub-section.

3.1 Methodology

Following Castro et al., (1990), observed spectral amplitude (acceleration) $U_{ij}(f, R_{ij})$, of EQ j, at recording station i, and frequency f can be modelled linearly as:

$$lnU_{ij}(f, R_{ij}) = lnM_i(f) + lnA(f, R_{ij}) \quad (1)$$

Here, $M_i(f)$ is a scalar, which depends on the size of the EQ (one value for each EQ). Further, $A(f, R_{ij})$ is the empirically determined attenuation function independent of the size of EQ, which incorporates both geometric spreading and anelastic attenuation variation with the hypocentral distance. It has to be mentioned here that $A(f, R_{ij})$ in Eq. (1) is not limited to a particular functional form, instead, is assumed to decay smoothly with hypocentral distance (R_{ij}) and take the value of unity at a reference distance (R_0), i.e., $A(f, R_0) = 1$ (Castro et al., 1990; 1996; 2003).

Model given by Eq. (1) does not contain any factor related to site effect. This site effect is absorbed in both $A(f, R_{ij})$ and $M_i(f)$ and hence any rapid undulations in $A(f, R_{ij})$ are due to this absorbed site effects (Oth et al., 2008). Two weighing factors, ω_1 and ω_2 are incorporated in the Eq. (1) following Castro et al., (1990). ω_2 is

Nat. Hazards Earth Syst. Sci. Discuss., https://doi.org/10.5194/nhess-2018-148
Manuscript under review for journal Nat. Hazards Earth Syst. Sci.
Discussion started: 10 July 2018

Natural Hazards and Earth System Sciences
Open Access
Discussions

used to smoothen the attenuation term with distance curve by supressing the undulations and there by removing any absorbed site effects from $A(f, R_{ij})$ and ω_2 is used to impose $A(f, R_0) = 1$ constraint, as mentioned earlier. The value of ω_1 and ω_2 is chosen reasonably such that the site effects are supressed and yet preserve the variations of the attenuation characteristics with distance (Oth et al., 2008). In the matrix form, following the notations of Menke (1989) and incorporating the weighting factors ω_1 and ω_2, Eq. (1) can be written in accordance with Castro et al., (1990) as:

$$
\begin{array}{ccc}
(A) & (X) & (b) \\
\left|\begin{array}{ccccc|ccccc|c}
1 & 0 & 0 & . & \ldots & 1 & 0 & 0 & . & \ldots & \\
0 & 1 & 0 & . & \ldots & 1 & 0 & 0 & . & \ldots & \\
. & . & . & . & \ldots & . & . & . & . & \ldots & \\
1 & 0 & 0 & . & \ldots & 0 & 1 & 0 & . & \ldots & \\
. & . & . & . & . & 0 & 1 & 0 & . & \ldots & \\
. & . & . & . & . & . & . & . & . & . & . \\
. & . & . & . & . & . & . & . & . & . & \\
\omega_1 & 0 & 0 & . & \ldots & . & . & . & . & \ldots & \\
-\omega_2/2 & \omega_2 & -\omega_2/2 & . & \ldots & . & . & . & . & \ldots & \\
0 & -\omega_2/2 & \omega_2 & -\omega_2/2 & \ldots & . & . & . & . & \ldots & \\
. & . & . & . & \ldots & . & . & . & . & \ldots &
\end{array}\right|
&
\left|\begin{array}{c}
\ln A_1 \\ . \\ . \\ . \\ \ln A_{10} \\ \\ \ln M_1 \\ . \\ . \\ . \\ \ln M_N
\end{array}\right|
\begin{array}{c}
\\ \\ \\ = \\ \\ \\ \\ \\ \\ \\ \\
\end{array}
&
\left|\begin{array}{c}
\ln U_{11} \\ . \\ . \\ \ln U_{ij} \\ . \\ \\ 0 \\ 0 \\ 0 \\ 0 \\ .
\end{array}\right|
\end{array}
$$

(2)

The hypocentral distances of the data set is discretized into number of bins of equal lengths and the value of $A(f, R_{ij})$ is computed at each bin. The lengths of the bins are selected such that there is almost equal number of data points in every bin. Further, $\ln A(f, R_{ij})$ versus hypocentral distance curves at each of the selected frequencies are computed solving Eq. (2) in a least square sense, using singular value decomposition method (Menke, 1989).

3.2 Spectral attenuation with distance

Figure 2 shows the number of EQ records for various hypocentral distance range considered. It can be observed from Figure 2 that there are very few EQ records available beyond 115km. For this reason, EQ records with hypocentral distance up to 115km are considered for the determination of path attenuation. The constraint $A(f, R_0) = 1$ is applied at R_0=15km, irrespective of the frequency. The hypocentral distance range from 15 to 115km is divided into 10 bins, each bin having 10km width. Further, attenuation curves are computed for each of the selected 17 frequencies from 1Hz to 15Hz (see Table 4, column 1). Variation of attenuation curves with hypocentral distance, obtained in the present study, for the selected frequencies can be depicted in Figure 3. Based on Figure 3, a general trend in which attenuation curves exhibit decay with distance up to 105km can be observed, beyond which a kink is observed. The kink in the attenuation curves beyond 105km is very distinct and clear at lower frequencies (<5.5 Hz). Bindi et al., (2004) and Oth et al., (2010) reported a similar trend in the attenuation curves for the Umbria Marche and Japan regions respectively. Oth et al., (2010) attributed this behaviour to the combined effect of reflected or refracted arrivals from the Moho in Japan. Presence of Moho in

Nat. Hazards Earth Syst. Sci. Discuss., https://doi.org/10.5194/nhess-2018-148
Manuscript under review for journal Nat. Hazards Earth Syst. Sci.
Discussion started: 10 July 2018

Natural Hazards and Earth System Sciences
Open Access
Discussions

the North-west Himalaya was reported by Saikia et al., (2016) based on Teleseismic receiver function analysis. The above discussions suggest that attenuation curves obtained in this study at larger distances may be influenced by reflected or refracted waves from the Moho. Observing the attenuation curves at different frequencies in Figure 3 can conclude that at higher frequency, attenuation curves decay more rapidly than at lower frequency. This observation is consistent with the findings by Castro et al., (2003) for the region of Guadeloupe, France and Oth et al., (2011) for the region of Japan.

Further, for the kink observed at 105km, in case of lower frequencies, its sharpness reduces with increasing frequency as can be observed in Figure 3. At frequencies greater than 10Hz, the kink at 105km smoothen and the attenuation curves beyond 105km for higher frequencies becomes flat as observed in Figure 3. This change in the character of the kink at higher frequency indicates that the arrival of waves from the Moho also gets attenuated more at higher frequencies compared to lower frequencies.

3.3 Quality factor estimation

In order to estimate Q_s, inversion is repeated, however only considering records within hypocentral distance in the range 15km to 105km, where a monotonic decrease in attenuation curves with distance is observed. The attenuation curves are modelled in terms of geometric spreading $[G(f, R_{ij}])$ and quality factor (Q) in accordance with Castro et al., (1996) as;

$$A(f, R_{ij}) = G(f, R_{ij}) \left[e^{\frac{-\pi \cdot f \cdot R_{ij}}{Q \cdot \beta}} \right] \qquad (3)$$

Where, f is the frequency and β is the mean shear wave velocity in the crustal medium taken as 3.5km/s as per Mukhopadhyay and Kayal, (2003). Further, $G(f, R_{ij})$ is considered as $1/R_{ij}$ in accordance with Banerjee and Kumar (2015) for this region. For each frequency considered in this study (see Table 4), Eq. (3) is linearized by taking logarithm and corrected for the effect of $G(f, R_{ij})$ as given in Eq. (4).

$$ln\, \mathrm{A}(\mathrm{f}, \mathrm{R}_{\mathrm{ij}}) - ln \mathrm{G}(\mathrm{f}, \mathrm{R}_{\mathrm{ij}}) = \frac{-\pi \cdot \mathrm{f}}{\mathrm{Q} . \beta} \mathrm{R}_{\mathrm{ij}} \qquad (4)$$

Ascribed to Castro et al., (2003), Eq. 4 is written in the form;

$$a(R) = -m\, R \qquad (5)$$

Where $a(R)$ and m are given as;

$$a(R) = lnA\big(f, R_{ij}\big) - ln\, G\big(f, R_{ij}\big) \qquad (6)$$

$$m = \frac{-\pi \cdot f}{Q \cdot \beta} \qquad (7)$$

Where, m in Eq. 5 is the slope of a linear least square fit obtained between $a(R)$ and R, for each of the selected frequencies. Further, the Q values are estimated for the selected frequencies by substituting the value of m computed using Eq. (7). Columns 2 and 3, Table 4 list the value of m and Q with frequency (f) respectively. In order to build the frequency dependent relationship $Q_s = Q_0\, f^n$, the value of Q is fitted as a function of frequency using a power law. In the above expression, n is the frequency dependent coefficient, which is approximately equal to 1 and varies on the basis of the heterogeneity of the medium (Aki 1980). Variation of Q against frequency as illustrated in Figure 4 gives frequency dependent Q_s for the North-west Himalaya as;

$$Q_s = 105\ f^{0.94} \tag{8}$$

The values of n and Q_0 (in the expression $Q_s = Q_0\ f^n$) are attributed to the level of tectonic activity and degree of heterogeneity respectively, present in the region. Aki (1980) concluded higher values of n for tectonically active regions in comparison to that of stable regions. Similarly, low value of Q_0 (<200) is an indication of larger degree of heterogeneities in the medium (Joshi 2006). The values of n (=0.94) and Q_0 (=104), obtained in this study indicates that the present study region is tectonically active, characterized by higher degree of heterogeneities, in accordance with Aki (1980) and Joshi (2006).

3.4 Comparison with Regional and Global Attenuation Characteristics

As discussed earlier, numerous studies exist where path attenuation of different parts of the present study area were attempted in the past. Comparison of present results with those obtained by the previous researchers for the NorthWest Himalaya and Delhi region are attempted as shown in Figure 5. It can be seen from Figure 5 that the attenuation curve obtained in the present study falls in between existing attenuation curves for the North-west Himalaya in the literature, [Kinnaur, (Kumar et al., 2009), Kumoan (Mukhopadhyay et al., 2010), Garhwal regions (Negi et al., 2015) and Delhi (Sharma et al., 2015)]. It has to be highlighted here that the data base for the present study includes EQ records from Kinnaur, Kumoan, Garhwal regions of North West Himalaya as well as from regions around Delhi. For this reason, the value of Q_0 and n obtained in the present study reflects an average attenuation of regions encompassing North-west Himalaya up to Delhi region.

Furthermore, the attenuation results obtained in this study is compared with some typical results obtained globally in terms of attenuation characteristics and tectonic setting as shown in Figure 6. Literature suggests low values of Q_s for tectonically active regions [e.g. Kato Japan region (Yoshimoto et al., 1993); East central Iran (Mahood et al., 2009); Egypt (Abdel 2009); and Umbria–Marche region (Lorenzo et al., 2013)]. Similarly, relatively high values of Q_s were found for tectonically stable areas [e.g. Baltic Shield (Kvamme and Havskov 1989); Central south Korea (Kim et al., 2004) and South Eastern Korea (Chung and Sato 2001)]. The attenuation values obtained in the present study show good agreement with other studies with lower value of Q_s. Further, attenuation curves for the present region is found closer to regions of high seismicity like Umbria–Marche and Eastern Iran as can be observed from Figure 6.

4 Site Effects

After estimation of path parameter as discussed in the previous section, site characteristics of recording stations are determined using the second step of inversion. In addition to GINV, site components are also estimated using HVSR method. Detailed discussion on GINV and HVSR is given in the subsequent sections.

4.1 GINV

The GINV was developed by Andrews (1986) by recasting the method of spectral ratio into a generalized inversion problem. Since then, various forms of this technique have been developed and used for estimating the

Nat. Hazards Earth Syst. Sci. Discuss., https://doi.org/10.5194/nhess-2018-148
Manuscript under review for journal Nat. Hazards Earth Syst. Sci.
Discussion started: 10 July 2018

Natural Hazards and Earth System Sciences
Open Access
Discussions

seismic characteristics by various researchers (Castro et al., 1990; Boatwright et al., 1991; Oth et al., 2008 etc.). The methodology used for estimating site characteristics in the present study is discussed here.

As per Iwata and Irikura (1988), the observed Fourier amplitude (acceleration) spectrum (FAS) of the i^{th} EQ recorded, at the j^{th} recording station, $U(f)_{ij}$ can be represented in the frequency domain as the product of source term ($S(f)_{ij}$), path attenuation ($A(f)_{ij}$) and site term ($G(f)_j$) as shown below;

$$U(f)_{ij} = S(f)_{ij}\, A(f)_{ij}\, G(f)_j \qquad (9)$$

Further, the path attenuation term can be removed from the spectral content of the record following Andrews (1986) as;

$$U^A(f)_{ij} = \frac{U(f)_{ij}}{A(f)_{ij}} = S(f)_{ij}\, G(f)_j \qquad (10)$$

The value of $A(f)_{ij}$ is estimated here using Eq. (3) and by considering Q_s as per Eq. (8), obtained in the earlier section. Eq. (10) can be linearized, by taking natural logarithms on both sides as per Andrews (1986) giving;

$$lnU^A(f)_{ij} = ln\, S(f)_i + ln\, G(f)_j \qquad (11)$$

Considering: $ln\, S_i = s_i(f)$, $ln\, G\,(f)_j = g(f)$ and $lnU^A(f)_{ij} = d_{ij}$, Eq. (11) in the matrix form can be written in accordance with Joshi et al., (2010) and following the notations of Menke (1989) as;

←	1st event		→		←	nth event		→	← Site effect→						
1	2	…	m		1	2	…	m	1	2	…	m			
1	0	…	0	…...	0	0		0	1	0	…	0	$s_1(f_1)$		$d_1(f_1)$
0	1		0	…...	0	0		0	0	1	…	0	:		:
:			:		:	:		:	:	:		:	:		:
:			:		:	:		:	:	:		:	:		:
0	0	0	1		0	0	…	0	0	0	…	1	$s_1(f_n)$		$d_1(f_m)$
													$s_n(f_1)$	=	
													:		
For nth earthquake													$s_n(f_n)$		$d_n(f_m)$
0	0	…	0	…..	1		…	0	1	0	…	0	$g(f_1)$		$d_n(f_m)$
0	0	…	0	…..	0	1	…	0	0	1	…	0	$g(f_2)$		:
:	:		:		:	:		:	:	:		:	:		:
:	:		:		:	:		:	:	:		:	:		:
0	0	…	0	…	0	0	…	1	0	0	…	1	$g(f_m)$		$d_n(f_m)$

(12)

The matrix form in Eq. (12) represents a purely indeterminate system since there are $(n + 1) \times m$ unknowns for '$m \times n$' data (here m is the number of sample frequency and n is the number of EQs recorded at a particular recording station). Further, Eq. (12) is solved using minimum norm inversion procedure similar to the work by Joshi et al., (2010), Harinarayan and Kumar (2017) to determine $g(f)_j$ at each of the selected recording stations.

Based on the above discussed methodology, inversions are performed for east-west, north-south and vertical components of EQ records separately to obtain the amplification curves in the frequency range of 0.25Hz to 15Hz for each of the three components. For further calculation, the horizontal component is obtained as the geometric mean of east-west and north-south components.

4.2 HVSR

HVSR method is an extension of Nakamura (1989) technique, which has been widely used in the recent years to assess the subsoil characteristics using recorded ambient noises. Nakamura (1989) technique is based on the assumption that the soil amplification effects are retained only in the horizontal component whereas the source and the path effects are maintained both in vertical as well as horizontal components of ground motion. Hence, the ratio of horizontal and vertical components gives an estimate of site amplification. Lermo and Chavez-Garccia (1993) extended Nakamura (1989) technique to S wave part of the accelerograms and studied the theoretical basis of the technique by numerical modelling of SV waves. Later, HVSR method was applied to EQ recordings worldwide (Luzi et al., 2011; Yaghmaei-Sabegh and Tsang 2011; Alessandro et al., 2012; Harinarayan and Kumar 2017, 2018 etc.) to obtain the site characteristics.

Comparative studies between HVSR and other methods of evaluating site parameters reported by Field and Jacob (1995), Parolai et al., (2004), Shoji and Kamiyama (2002) Harinarayan and Kumar (2017) etc. show that, HVSR can provide good and reliable estimate of predominant frequency in the site amplification function. However, the above literatures also point out discrepancies in amplification levels obtained from HVSR with other methods. In order to compare the site amplification functions obtained from HVSR and GINV methods, HVSR for each station are computed considering the same S wave window as used in the GINV method. In the present work, HVSR for each recording station is determined using the following steps;

1. Calculate the FAS for the three components (north-south, east-west and vertical) of ground motion records.
2. Obtain the geometric mean of the two horizontal response spectra components (H) using Eq. (13) given below;

$$\mathrm{H} = (\mathrm{H_{EW}} \times \mathrm{H_{NS}})^{0.5} \tag{13}$$

3. Calculate the ratio of H to V (H/V).

Where, $\mathrm{H_{EW}}$ and $\mathrm{H_{NS}}$ are the FAS of the horizontal east-west and north-south components respectively and V is the FAS of the corresponding vertical component. Then, the HVSR at each recording station can be determined as;

$$(\mathrm{HVSR})_i = \frac{\sum_{i=1}^{\mathrm{Ni}} \frac{\mathrm{H}}{\mathrm{V}}}{\mathrm{N}_i} \tag{14}$$

Here, N_i is the number of events recorded at recording station "i" and $(\mathrm{HVSR})_i$ indicates the average HVSR value for a particular station "i". The $\mathrm{f_{peak}}$ is the value of frequency corresponding to a maximum value of HVSR_i (denoted by $\mathrm{A_{peak}}$) at the recording station "i".

4.3 Site Parameters

Nat. Hazards Earth Syst. Sci. Discuss., https://doi.org/10.5194/nhess-2018-148
Manuscript under review for journal Nat. Hazards Earth Syst. Sci.
Discussion started: 10 July 2018

Natural Hazards and Earth System Sciences
Discussions

Site amplification curves are developed using GINV for the horizontal (GINV H) and the vertical components (GINV V). Figure 7 shows typical amplification curves obtained for GINV H (indicated by dashed lines) and GINV V (indicated by firm lines) at 6 stations. In general, obtained amplification value for GINV H is greater than GINV V for all frequencies. A typical observation (from Figure 7) for both GINV H and GINV V is that the high level of amplification is observed at high frequencies. For several recording stations, clear and distinct peak in the amplification curve can be observed (eg. JAMI, BAR, GHA and SND) from Figure 7. Moreover, the main peaks of the GINV V component are usually at higher frequencies than for the GINV H component. Further, in the case of few recording stations, the shift in frequency is relatively close to a factor $\sqrt{2}$ (eg. BAR and GHA). Next, Site amplification factor (SAF) is estimated based on the GINV results (denoted by GINV H/V) as the ratio of GINV H to GINV V. The value of frequency corresponding to the maximum value of SAF (denoted as A_{peak}) is f_{peak}. GINV H/V curves are compared with those estimated using HVSR method for a total of 101 recording stations. Figure 8 shows the comparison of the HVSR (indicated by dashed lines) and GINV H/V (indicated by firm line) for 9 recording stations that provide a good sample of typically observed effects for all the recording stations in the present study. A general observation made from Figure 8 is that both HVSR and GINV H/V show similar SAF patterns for all recoding stations in the studied frequency range. Overall value of f_{peak} obtained exhibit 1:1 matching between the two methods. However, there is trend of difference in terms of A_{peak} values. A_{peak} values obtained using HVSR are found higher compared to those obtained using GINV H/V curves. This observation was also reported by many studies in other regions (Sharma et al., 2014; Field and Jacob, 1995). The values of f_{peak} obtained using GINV H/V and HVSR are tabulated in Column 5 and 7, Table 1. Similarly, the values of A_{peak} obtained using GINV H/V and HVSR are tabulated in Column 6 and 8, Table 1. The maximum value of f_{peak} of 15Hz is observed for the recording station GGI with a value of A_{peak} of 5.3. The maximum value of A_{peak} of 12.2, based on GINV H/V is observed for ADIB recording station at 6.3Hz. The range of A_{peak} based on HVSR varies between 1.7 and 19.4, while based on GINV H/V, the range of A_{peak} varies between 1.5 and 12.7. The range of f_{peak} based on HVSR varies between 0.4Hz and 10Hz, while based on GINV H/V, the range of f_{peak} varies between 0.5Hz and 15Hz.

Further, based on the value of f_{peak} obtained using GINV, the recording stations are classified as either rock sites or soil sites. In general, criteria based on average shear wave velocity over 30m (V_{s30}) is used for site classification. A site can also be classified based on f_{peak} values. Such an approach was used by Harinarayan and Kumar (2017) to classify the recording stations in the North-West Himalaya based on f_{peak} obtained using HVSR method, where stations having f_{peak} less than 6.35Hz were classified as soil sites and stations having f_{peak} greater than 6.35Hz were classified as rock sites. The range of f_{peak} values reported by Harinarayan and Kumar (2017) for soil and rock sites were calculated based on the range of V_{s30} based on NEHRP site classification scheme in accordance with the Eq. (15) (Kramer, 1996), correlating f_{peak} to soil depth (denoted by H and taken as 30m) and shear wave velocity (V_z).

$$f_{peak} = {V_z}/{4H} \tag{15}$$

Based on this classification criteria, all the recording stations in the present are classified as either rock site or soil site and is given in Column 9 of Table 1. Out of 101 recording stations 10 recording stations are classified as rock sites and the rest 91 stations are classified as soil sites.

Nat. Hazards Earth Syst. Sci. Discuss., https://doi.org/10.5194/nhess-2018-148
Manuscript under review for journal Nat. Hazards Earth Syst. Sci.
Discussion started: 10 July 2018

4.4 Spatial distribution of GINV H/V characteristics

To provide further insight into the GINV results, distribution of f_{peak} (Fig. 9) and A_{peak} (Fig. 10) over the region confined by the Delhi, Himachal Pradesh, Haryana, Uttarakhand and Punjab are developed separately. Considering the distribution of f_{peak} for the Delhi region (Figure 9A), an increasing trend from west to east with a range of 2 to 3Hz in the western region and 3 to 4.67Hz in the eastern region is observed. Spatial distribution of A_{peak} for the Delhi region (Figure 10A) reveals A_{peak} in the range 2 to 3 in the western region. For the state of Haryana, the values of f_{peak} and A_{peak}, in general, are found to be in the range of 1 to 5.3Hz and 2 to 4 (see Figures 9B and 10B respectively). For the state of Himachal Pradesh spatial distribution of f_{peak} (Fig 9C) shows an increasing trend from south to north with a range of 3 to 4.67Hz in the northern region and 1.5 to 3Hz in the southern region. The value of A_{peak} for the Himachal Pradesh in the range 1.8 to 6.2. For the state of Punjab, the spatial distribution of f_{peak} (Figure 9D) shows a decreasing trend from east (3Hz) to west (1.5Hz) whereas, an increasing trend is observed form the east (3 to 5) to west (2 to 3) in the case of A_{peak} values. The range of f_{peak} for the state of Uttarakhand varies from 0.5 to 5Hz, and A_{peak} varies from 1.5 to 6.5 (Figure 9E and 10E). The spatial variation of A_{peak} for the region of Uttarakhand shows an increasing trend from north to south. The spatial distribution of A_{peak} and f_{peak} discussed above and shown in Fig 9 and Fig. 10 can be useful for regional seismic hazard analysis.

4.5 Relationship between GINV H/V results and V_{s30}

The value of V_{s30} are available for 8 recording stations in Terai region of Uttarakhand and 19 stations in Delhi region from Pandey et al., (2016a) and Pandey et al., (2016b) respectively based on results of MASW test. The values of V_{s30} for a total of 27 recording stations in Terai region of Uttarakhand and Delhi regions coincides with recording stations where A_{peak} and f_{peak} are determined in the present study. The values of V_{s30} (obtained from Pandey et al., 2016 a, b) and f_{peak} and A_{peak} (as per present work) for above 27 recording stations are listed in Table 5. Based on the present findings, relationship between f_{peak} and V_{s30} for the 27 recording stations is proposed as shown in Figure 11a with an R^2 value of 0.71 as:

$$\log \mathrm{V}_{s30} = (0.48)\left(\log \mathrm{f}_{\mathrm{peak}}\right) + (2.33) \qquad (16)$$

Similarly, the relationship between A_{peak} and V_{s30} for above 27 recording stations, as obtained in the present study is shown in Figure 11b is as follows:

$$\log V_{s30} = -(0.74)\left(\log A_{peak}\right) + (2.93) \qquad (17)$$

A lack of correlation (correlation coefficient =0.47) between V_{s30} and A_{peak} is observed as shown in Figure 11B, which is also reported in the previous studies like Dutta et al., (2001), (2003) and Hassani et al., (2011). It can be concluded from the proposed correlations (Eqs. 16 and 17) that the value of f_{peak} increases with increase in V_{s30} whereas the value of A_{peak} decreases with the increase in the value of V_{s30}. It has to be highlighted here that both the equations [Eqs. 16 and 17] are applicable for sites having f_{peak} in the range 1.8 to 6 Hz, and A_{peak} in the range 2 to 6.9.

Nat. Hazards Earth Syst. Sci. Discuss., https://doi.org/10.5194/nhess-2018-148
Manuscript under review for journal Nat. Hazards Earth Syst. Sci.
Discussion started: 10 July 2018

Natural Hazards and Earth System Sciences
Discussions

Conclusion

The strong motion recordings available in PESMOS databank from 2004 to 2016 for the North-west Himalaya and its surrounding areas are separately analysed to determine the path attenuation and site parameters using a two-step inversion procedure. In the first step of inversion, non-parametric attenuation curves have been developed. The attenuation with hypocentral distance shows a kink around 105km indicating the presence of reflected and refracted arrival from the Moho discontinuity. At hypocentral distance less than 105km, the attenuation curves decreases monotonically with distance. The S wave quality factor for distances less than 105km is described well as a function of frequency as: $Q_s = 105\, f^{0.94}$. The values of n (=0.94) and Q_0 (=104) obtained in the present study indicates the region to be heterogeneous and seismically active. The $Q_s$obtained in this study is comparable with those estimated in various regions of North West Himalaya and Delhi NCR region. Further, the attenuation characteristics of S waves in the present study are found close to other similar and seismically active regions of the world.

In the second step of inversion, amplification curves for horizontal and vertical components are computed and SAF for all 101 recording stations are estimated. The value of f_{peak} and A_{peak} obtained from the SAF curves are in the range of 0.5 to 15Hz and 1.5 to 12.7 respectively. SAF are also estimated using HVSR method and general comparison between the two methods shows similarities in terms of the general shape and the value of f_{peak}, even though there is difference in the values of A_{peak}. Further, the recording stations are classified as rock site or soil site based on the values of f_{peak}. Out of 101 recording stations 10 stations are classified as rock sites and 91 stations are classified as soil sites. Further, based on the values of f_{peak} and A_{peak} spatial distribution maps for the states of Delhi, Haryana, Himachal Pradesh, Uttarakhand and Punjab have been developed separately.

In conclusion, the path and site parameters found in this study provide important elements for further strong motion simulations and seismic hazard assessment. Identifying recording station on rock sites enables to utilize PESMOS data base for inversion studies requiring reference site, especially for computing EQ source parameters.

Authors Contribution:

Harinarayan N H developed code generalized inversion, analyzed the records and all relevant literature review. Kumar Abhishek (AK) highlighted the importance of site characterization for PESMOS recording stations and need for the study.

Acknowledgement

The authors would like to thank the INSPIRE Faculty program by the Department of Science and Technology (DST), Government of India for the funding project ‘‘Propagation path characterization and determination of in-situ slips along different active faults in the Shillong Plateau’’ ref. no. DST/INSPIRE/04/2014/002617 [IFA14-ENG-104] for providing necessary funding and motivation for the study.

Reference

Nat. Hazards Earth Syst. Sci. Discuss., https://doi.org/10.5194/nhess-2018-148
Manuscript under review for journal Nat. Hazards Earth Syst. Sci.
Discussion started: 10 July 2018

Natural Hazards and Earth System Sciences
Open Access
Discussions

Abdel-Fattah, A. K. (2009). Attenuation of body waves in the crust beneath the vicinity of Cairo Metropolitan area (Egypt) using coda normalization method. Geophysical Journal International, 176(1), 126-134.

Aki, K. (1980). Attenuation of shear-waves in the lithosphere for frequencies from 0.05 to 25 Hz. Physics of the Earth and Planetary Interiors, 21, 50–60.

Ameri, G., Oth, A., Pilz, M., Bindi, D., Parolai, S., Luzi, L & Cultrera, G. (2011). Separation of source and site effects by generalized inversion technique using the aftershock recordings of the 2009 L'Aquila earthquake. Bulletin of Earthquake Engineering, 9(3), 717-739.

Andrews, D. J. (1986). Objective determination of source parameters and similarity of earthquakes of different size. Earthquake source mechanics, 259-267.

Bilham, Roger, Kristine Larson, and Jeffrey Freymueller. "GPS measurements of present-day convergence across the Nepal Himalaya." *Nature* 386.6620 (1997): 61.

Bindi, D., Pacor, F., Luzi, L., Massa, M., & Ameri, G. (2009). The M w 6.3, 2009 L'Aquila earthquake: source, path and site effects from spectral analysis of strong motion data. Geophysical Journal International, 179(3), 1573-1579.

Castro, R. R., Anderson, J. G., & Singh, S. K. (1990). Site response, attenuation and source spectra of S waves along the Guerrero, Mexico, subduction zone. Bulletin of the Seismological Society of America, 80(6A), 1481-1503.

Castro, R. R., Fabriol, H., Bour, M., & Le Brun, B. (2003). Attenuation and site effects in the region of Guadeloupe, Lesser Antilles. Bulletin of the Seismological Society of America, 93(2), 612-626.

Castro, R. R., Pacor, F., Sala, A., & Petrungaro, C. (1996). S wave attenuation and site effects in the region of Friuli, Italy. Journal of Geophysical Research: Solid Earth, 101(B10), 22355-22369.

Chung, T. W., & Sato, H. (2001). Attenuation of high-frequency P and S waves in the crust of southeastern South Korea. Bulletin of the Seismological Society of America, 91(6), 1867-1874.

De Lorenzo, S., Del Pezzo, E., & Bianco, F. (2013). Qc, Qβ, Qi and Qs attenuation parameters in the Umbria–Marche (Italy) region. *Physics of the Earth and Planetary Interiors*, *218*, 19-30.

Harinarayan, N. H., & Kumar, A (2017). Seismic Site Classification of Recording Stations in Tarai Region of Uttarakhand, from Multiple Approaches. *Geotechnical and Geological Engineering*, 1-16.

Harinarayan, N. H., & Kumar, A. (2018). Determination of NEHRP Site Class of Seismic Recording Stations in the Northwest Himalayas and Its Adjoining Area Using HVSR Method. Pure and Applied Geophysics, 175(1), 89-107.

Hartzell, S. H. (1992). Site response estimation from earthquake data. Bulletin of the Seismological Society of America, 82(6), 2308-2327.

Joshi, A. (2006). Use of acceleration spectra for determining the frequency-dependent attenuation coefficient and source parameters. *Bulletin of the Seismological Society of America*, *96*(6), 2165-2180.

Nat. Hazards Earth Syst. Sci. Discuss., https://doi.org/10.5194/nhess-2018-148
Manuscript under review for journal Nat. Hazards Earth Syst. Sci.
Discussion started: 10 July 2018

Natural Hazards and Earth System Sciences
Open Access
Discussions

Joshi, A., Mohanty, M., Bansal, A. R., Dimri, V. P., & Chadha, R. K. (2010). Use of spectral acceleration data for determination of three-dimensional attenuation structure in the Pithoragarh region of Kumaon Himalaya. Journal of seismology, 14(2), 247-272.

Kim, K. D., Chung, T. W., & Kyung, J. B. (2004). Attenuation of high-frequency P and S waves in the crust of Choongchung provinces, central South Korea. Bulletin of the Seismological Society of America, 94(3), 1070-1078.

Konno, K., & Ohmachi, T. (1998). Ground-motion characteristics estimated from spectral ratio between horizontal and vertical components of microtremor. Bulletin of the Seismological Society of America, 88(1), 228-241.

Kumar, A., Mittal, H., Sachdeva, R., & Kumar, A. (2012). Indian strong motion instrumentation network. Seismological Research Letters, 83(1), 59-66.

Kumar, N., Sharma, J., Arora, B. R., & Mukhopadhyay, S. (2009). Seismotectonic model of the Kangra–Chamba sector of northwest Himalaya: Constraints from joint hypocenter determination and focal mechanism. Bulletin of the Seismological Society of America, 99(1), 95-109.Menke, W. (2012). Geophysical data analysis: discrete inverse theory: MATLAB edition (Vol. 45). Academic press

Kvamme, L. B., & Havskov, J. (1989). Q in southern Norway. Bulletin of the seismological society of america, 79(5), 1575-1588.

Ma'hood, M., Hamzehloo, H., & Doloei, G. J. (2009). Attenuation of high frequency P and S waves in the crust of the East-Central Iran. Geophysical Journal International, 179(3), 1669-1678.

Mukhopadhyay, S., Sharma, J., Del-Pezzo, E., & Kumar, N. (2010). Study of attenuation mechanism for Garwhal–Kumaun Himalayas from analysis of coda of local earthquakes. Physics of the Earth and Planetary Interiors, 180(1-2), 7-15.

Nath, S. K., Sengupta, P., & Kayal, J. R. (2002). Determination of S-wave site response in the Garhwal Himalaya from the aftershock sequence of the 1999 Chamoli earthquake. Bulletin of the Seismological Society of America, 92(3), 1072-1081.

Negi, S. S., Paul, A., & Joshi, A. (2015). Body wave crustal attenuation characteristics in the Garhwal Himalaya, India. Pure and Applied Geophysics, 172(6), 1451-1469.

Oth, A., Bindi, D., Parolai, S., & Di Giacomo, D. (2011). Spectral Analysis of K-NET and KiK-net Data in Japan, Part II: On Attenuation Characteristics, Source Spectra, and Site Response of Borehole and Surface StationsSpectral Analysis of K-NET and KiK-net Data in Japan, Part II. Bulletin of the Seismological Society of America, 101(2), 667-687.

Oth, A., Bindi, D., Parolai, S., & Wenzel, F. (2008). S-wave attenuation characteristics beneath the Vrancea region in Romania: new insights from the inversion of ground-motion spectra. Bulletin of the Seismological Society of America, 98(5), 2482-2497.

Oth, A., Parolai, S., Bindi, D., & Wenzel, F. (2009). Source spectra and site response from S waves of intermediate-depth Vrancea, Romania, earthquakes. Bulletin of the Seismological Society of America, 99(1), 235-254.

Philip, G., Suresh, N., & Bhakuni, S. S. (2014). Active tectonics in the northwestern outer Himalaya: evidence of large-magnitude palaeoearthquakes in Pinjaur Dun and the Frontal Himalaya. Current Science, 106, 211–222.

Saikia, S., Chopra, S., Baruah, S., Baidya, P. R., & Singh, U. K. (2016). Crustal imaging of the Northwest Himalaya and its foredeep region from teleseismic events. Geomatics, Natural Hazards and Risk, 7(4), 1265-1286.

Sharma, B., Chingtham, P., Sutar, A. K., Chopra, S., & Shukla, H. P. (2015). Frequency dependent attenuation of seismic waves for Delhi and surrounding area, India. Annals of Geophysics, 58(2), 0216.

Sharma, J., Chopra, S., & Roy, K. S. (2013). Estimation of source parameters, quality factor (QS), and site characteristics using accelerograms: Uttarakhand Himalaya region. Bulletin of the Seismological Society of America, 104(1), 360-380.

Singh, C., Singh, A., Bharathi, V. S., Bansal, A. R., & Chadha, R. K. (2012). Frequency-dependent body wave attenuation characteristics in the Kumaun Himalaya. Tectonophysics, 524, 37-42.

Srivastava, H. N., Bansal, B. K., & Verma, M. (2013). Largest earthquake in Himalaya: An appraisal. Journal of the Geological Society of India, 82, 15–22.

Tripathi, J. N., Singh, P., & Sharma, M. L. (2014). Attenuation of high-frequency P and S waves in Garhwal Himalaya, India. Tectonophysics, 636, 216-227.

Valdiya, K.S. 1984. Aspects of Tectonics, Focus on south-central Asia. Tata McGraw-Hill Publishing Company Ltd., New Delhi, 319p.

Yoshimoto, K., Sato, H., & Ohtake, M. (1993). Frequency-dependent attenuation of P and S waves in the Kanto area, Japan, based on the coda-normalization method. Geophysical Journal International, 114(1), 165-174.

Nat. Hazards Earth Syst. Sci. Discuss., https://doi.org/10.5194/nhess-2018-148
Manuscript under review for journal Nat. Hazards Earth Syst. Sci.
Discussion started: 10 July 2018

502 **FIGURES**

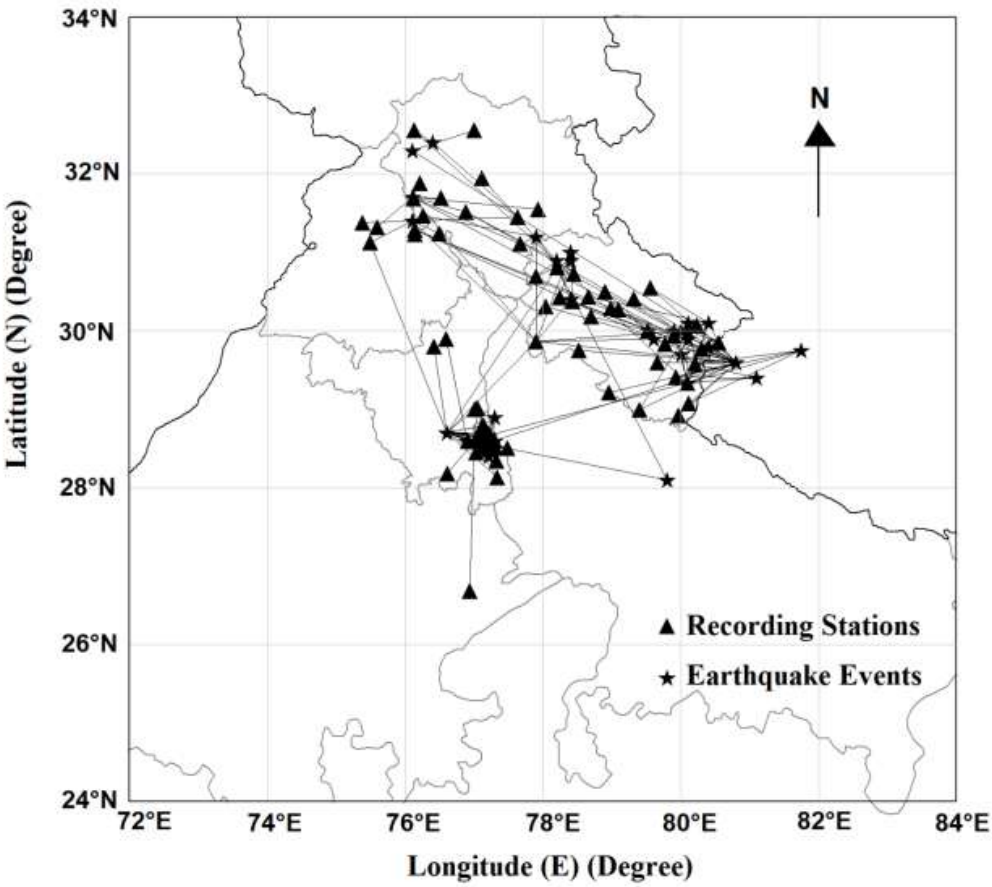

503
504 **Figure 1: Map of the region under study with EQs (stars), recording stations (triangles), and paths (solid-lines).**

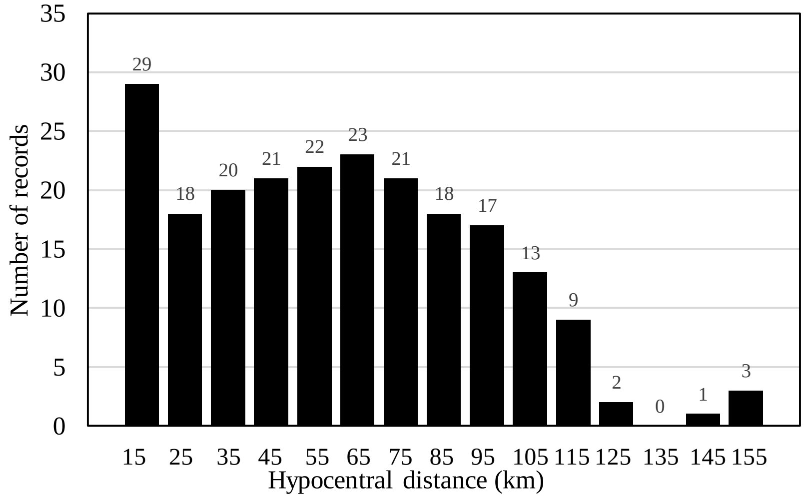

505
506 **Figure 2: Distribution of hypocentral distances in the data set.**

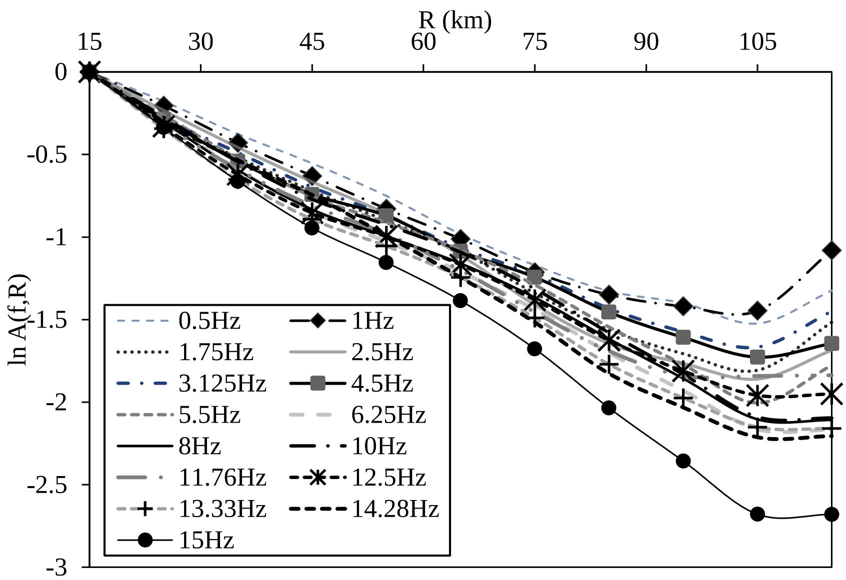

507
508 **Figure 3: S wave spectral attenuation versus hypocentral distance. Note that ln A(f,R$_0$) at reference distance is zero.**

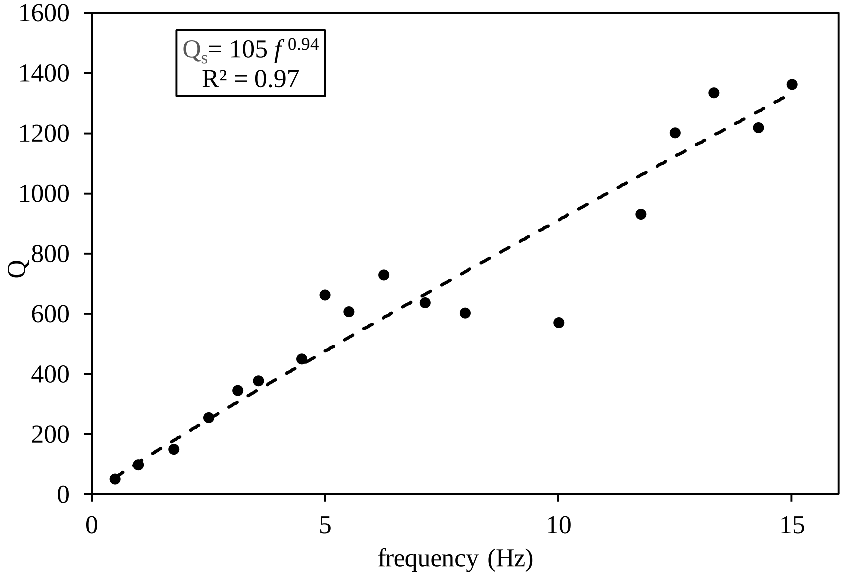

Figure 4: Frequency dependence of the quality factor Q for hypocentral distances between 15 km to 105 km

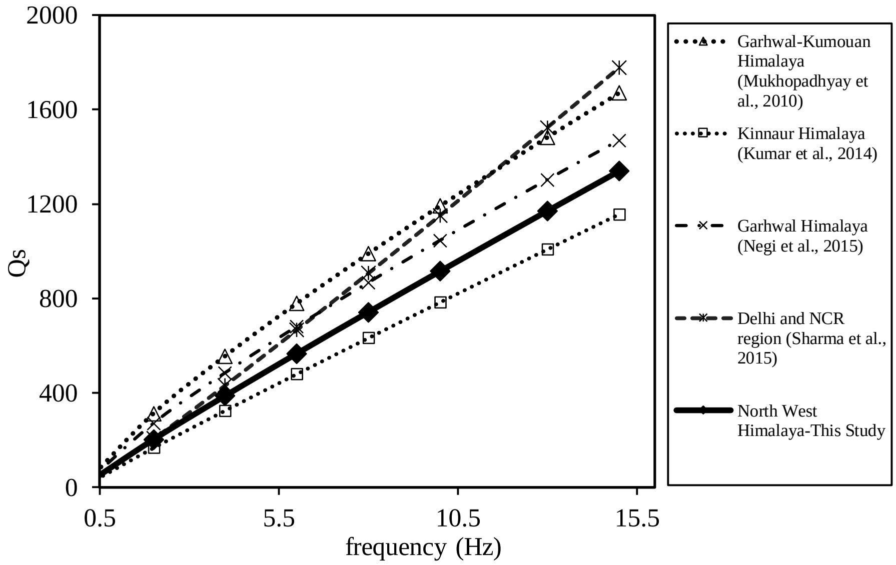

Figure 5: Comparison of Q_S values of North West Himalaya with those obtained from parts of North West Himalaya and Delhi region. The compared relations for Qs versus frequency are as follows: Garhwal-Kumouan Himalaya: $Q_S = 175 * f^{0.833}$ (Mukhopadhyay et al., 2010); Kinnaur Himalaya: $Q_S = 86 * f^{0.96}$ (Kumar et al., 2014) ; Garhwal Himalaya: $Q_S = 151 * f^{0.84}$ (Negi et al., 2015); Delhi and NCR region: $Q_S = 98 * f^{1.07}$ (Sharma et al., 2015).

Nat. Hazards Earth Syst. Sci. Discuss., https://doi.org/10.5194/nhess-2018-148
Manuscript under review for journal Nat. Hazards Earth Syst. Sci.
Discussion started: 10 July 2018

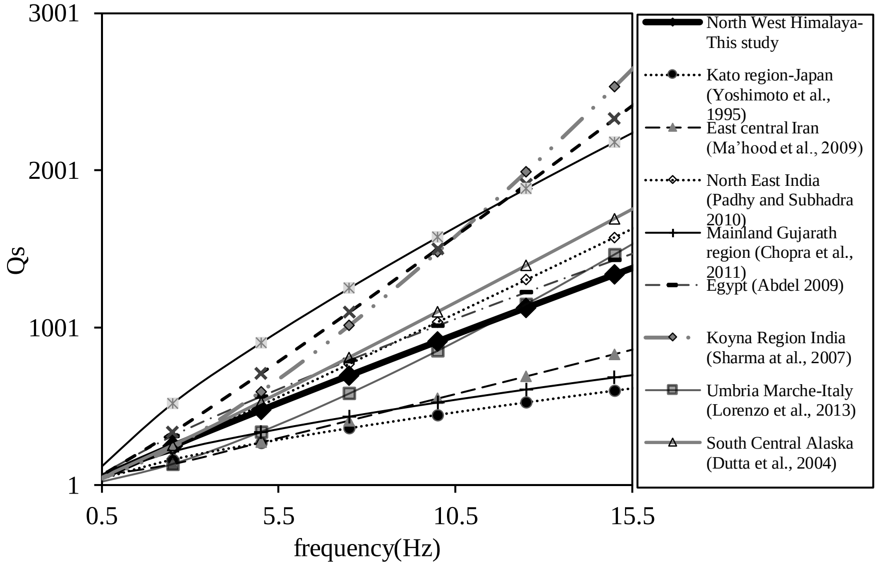

517

518 **Figure 6: Comparison of Q_S values of this study with regions of different tectonic settings of the world.**

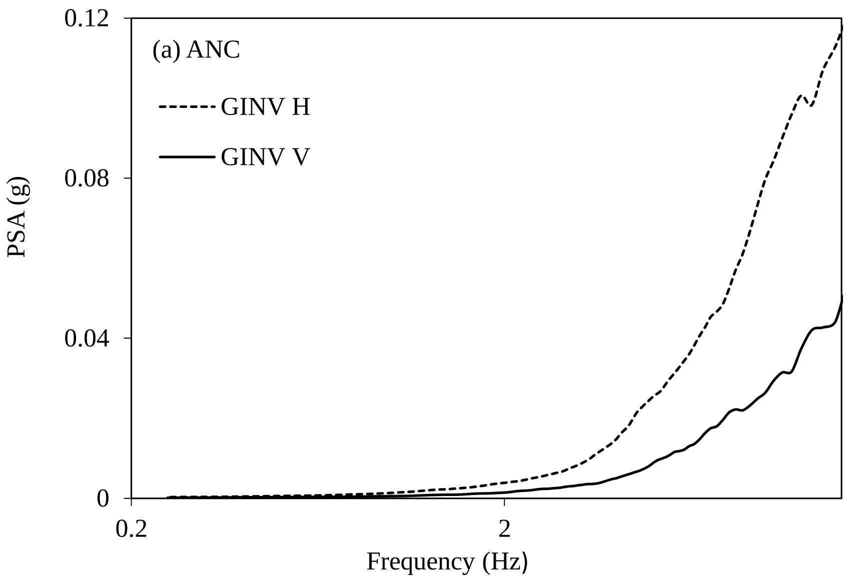

519

Nat. Hazards Earth Syst. Sci. Discuss., https://doi.org/10.5194/nhess-2018-148
Manuscript under review for journal Nat. Hazards Earth Syst. Sci.
Discussion started: 10 July 2018

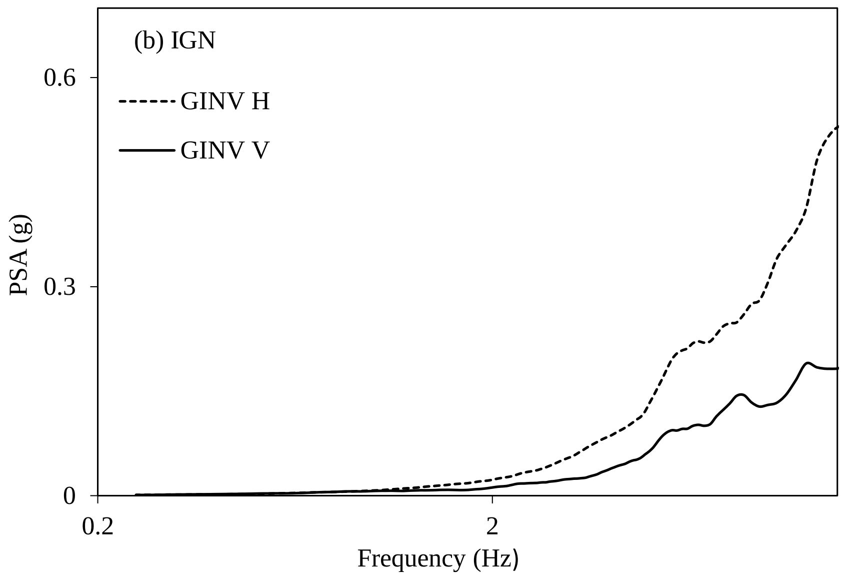

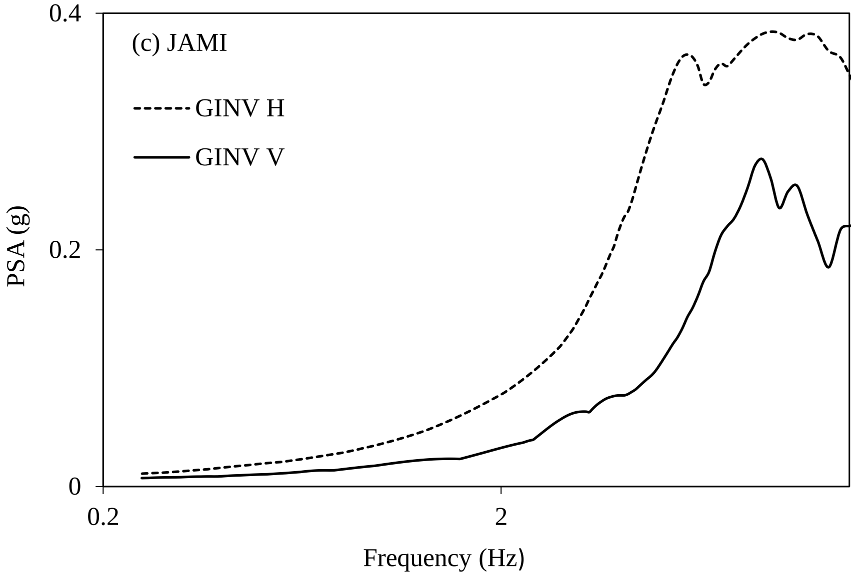

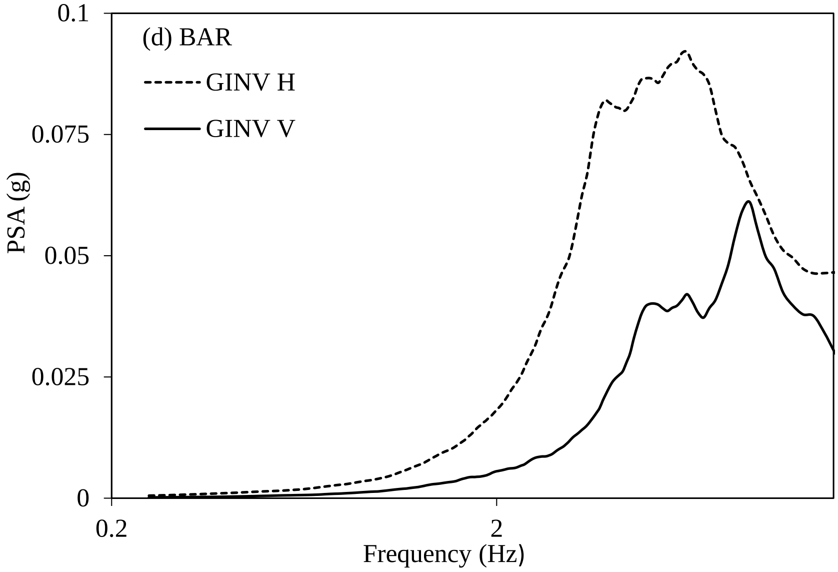
(d) BAR
GINV H
GINV V
PSA (g)
0.1
0.075
0.05
0.025
0
0.2
2
Frequency (Hz)

522

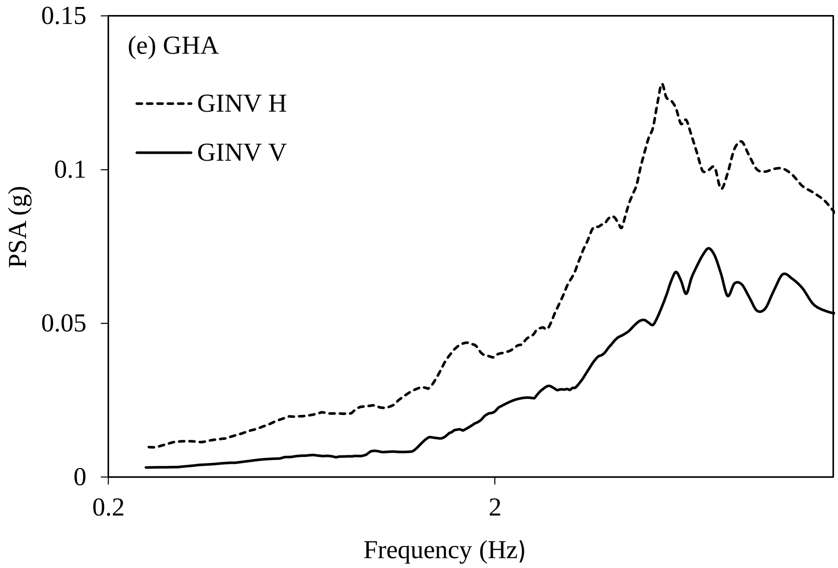
(e) GHA
GINV H
GINV V
PSA (g)
0.15
0.1
0.05
0
0.2
2
Frequency (Hz)

523

Nat. Hazards Earth Syst. Sci. Discuss., https://doi.org/10.5194/nhess-2018-148
Manuscript under review for journal Nat. Hazards Earth Syst. Sci.
Discussion started: 10 July 2018

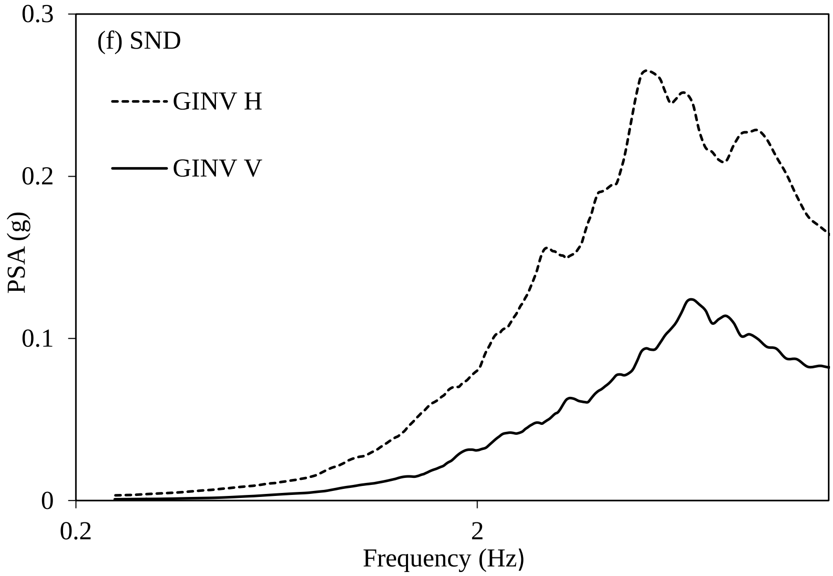

524
525 **Figure 7 (a-f). Site amplification curves obtained using GINV for horizontal component and vertical component**

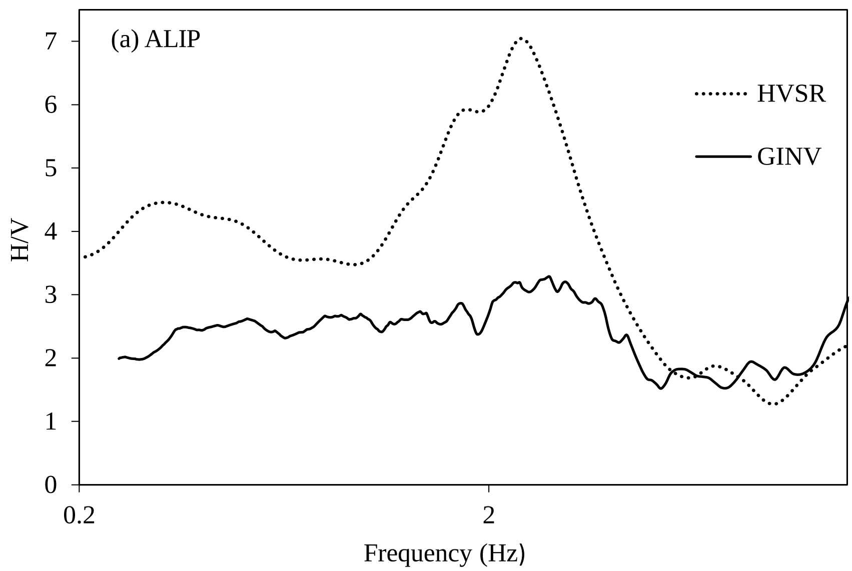

526

Nat. Hazards Earth Syst. Sci. Discuss., https://doi.org/10.5194/nhess-2018-148
Manuscript under review for journal Nat. Hazards Earth Syst. Sci.
Discussion started: 10 July 2018

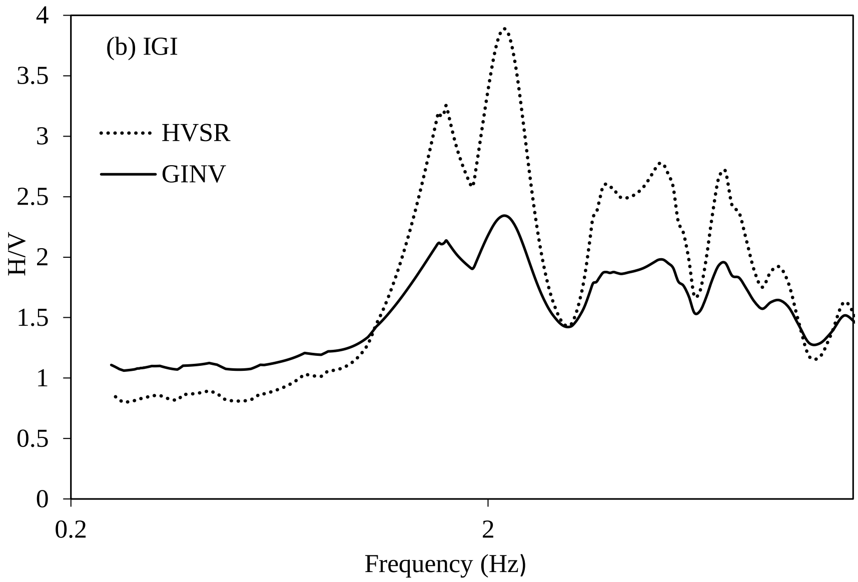

527

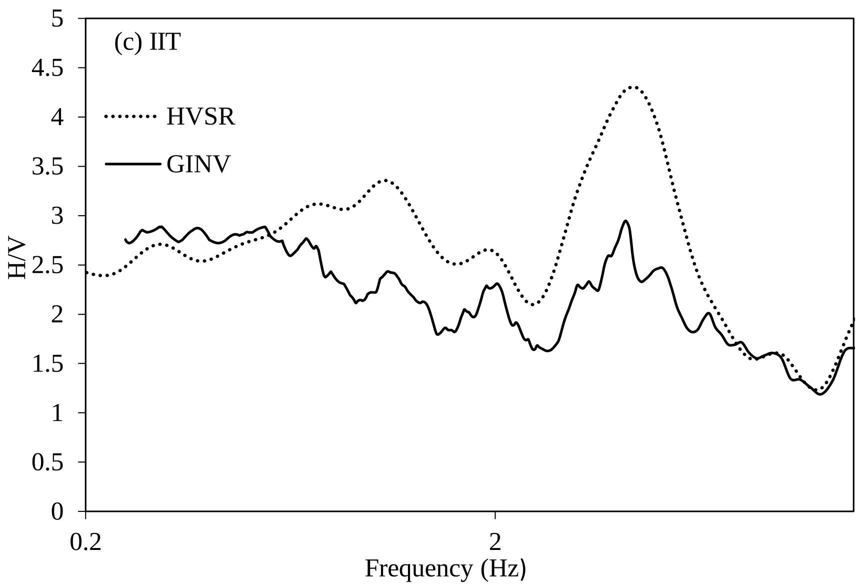

528

Nat. Hazards Earth Syst. Sci. Discuss., https://doi.org/10.5194/nhess-2018-148
Manuscript under review for journal Nat. Hazards Earth Syst. Sci.
Discussion started: 10 July 2018

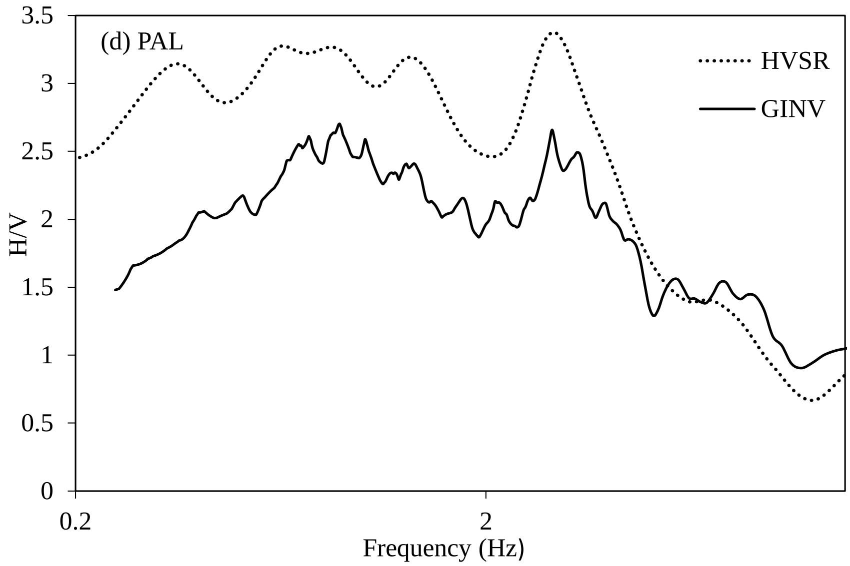

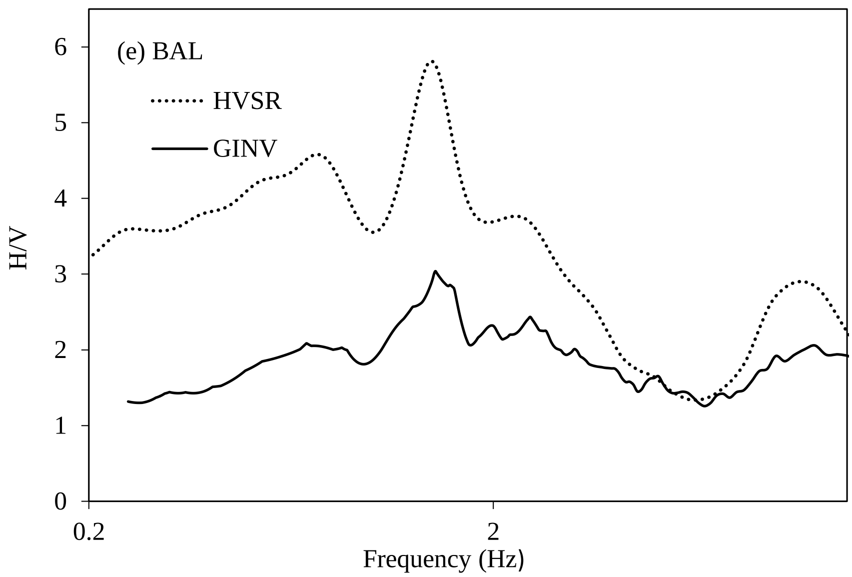

Nat. Hazards Earth Syst. Sci. Discuss., https://doi.org/10.5194/nhess-2018-148
Manuscript under review for journal Nat. Hazards Earth Syst. Sci.
Discussion started: 10 July 2018

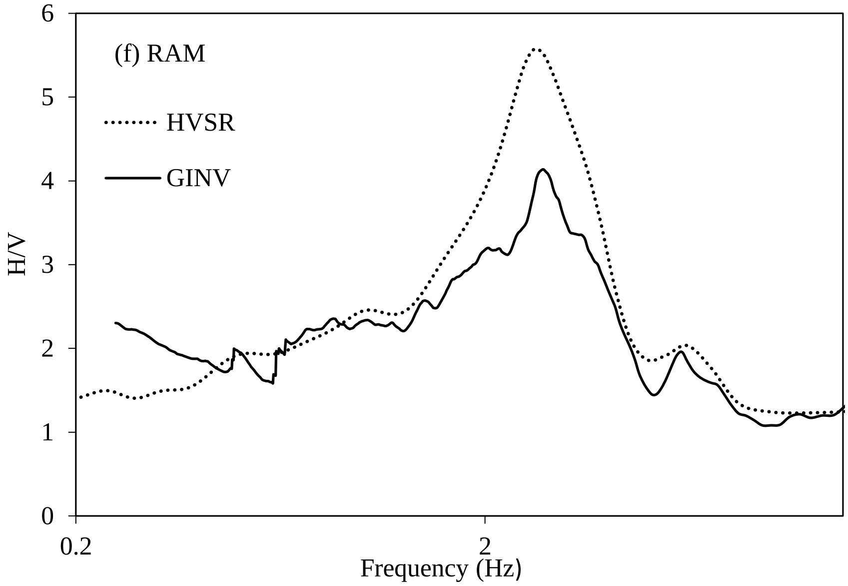

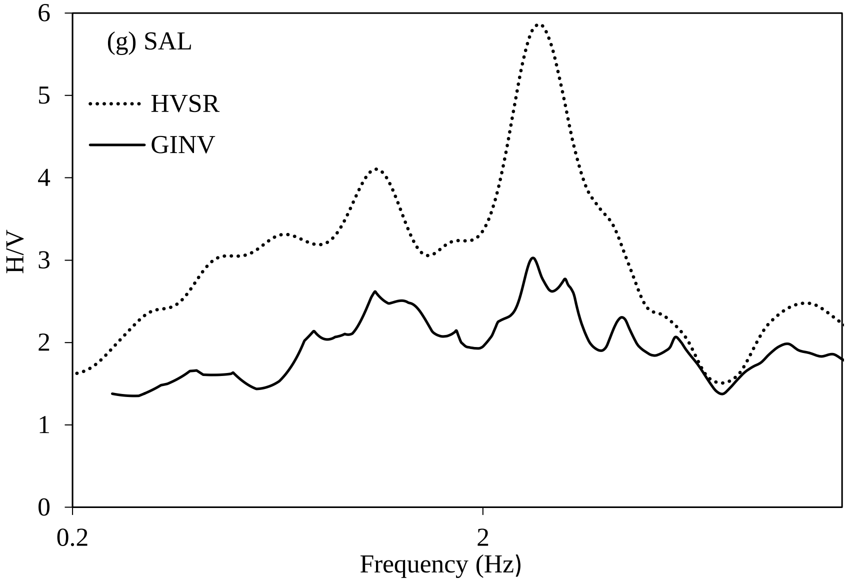

Nat. Hazards Earth Syst. Sci. Discuss., https://doi.org/10.5194/nhess-2018-148
Manuscript under review for journal Nat. Hazards Earth Syst. Sci.
Discussion started: 10 July 2018

Natural Hazards and Earth System Sciences
Open Access
Discussions

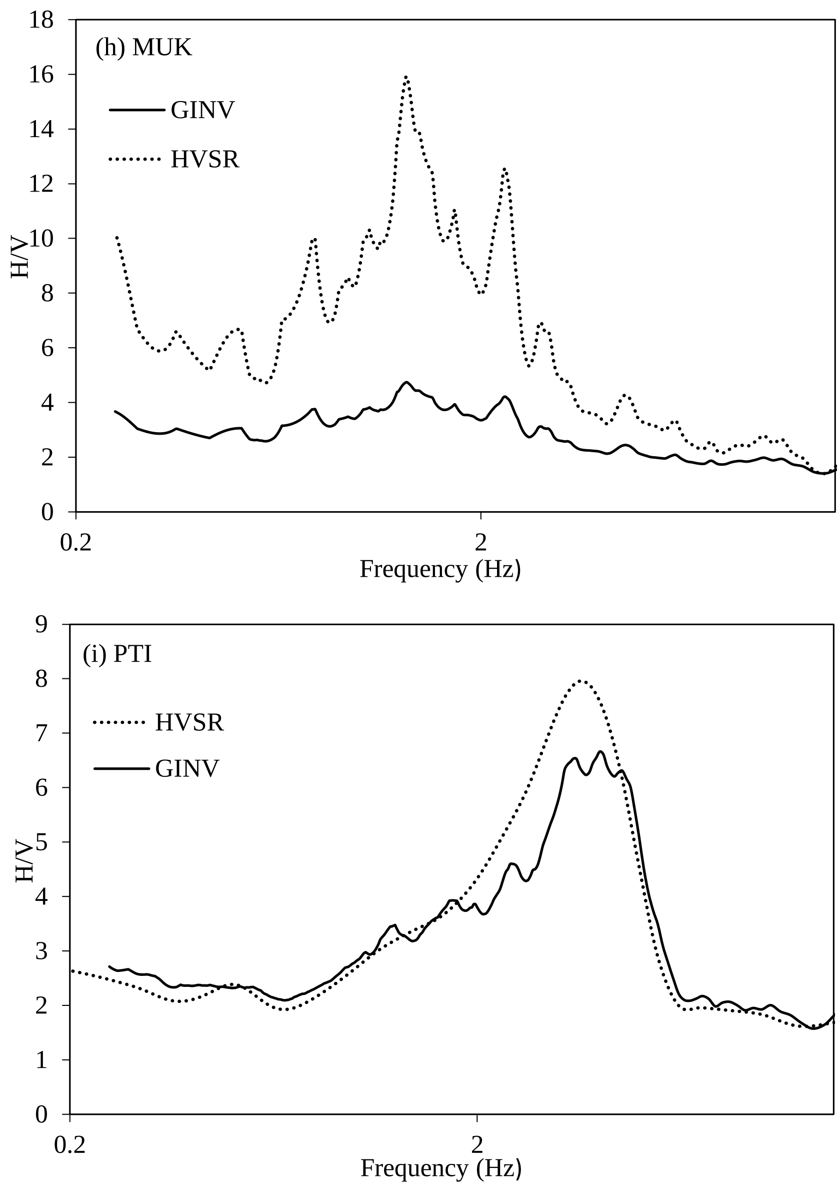

Figure 8 (a-i): Horizontal to vertical ratio curve obtained using GINV and HVSR method.

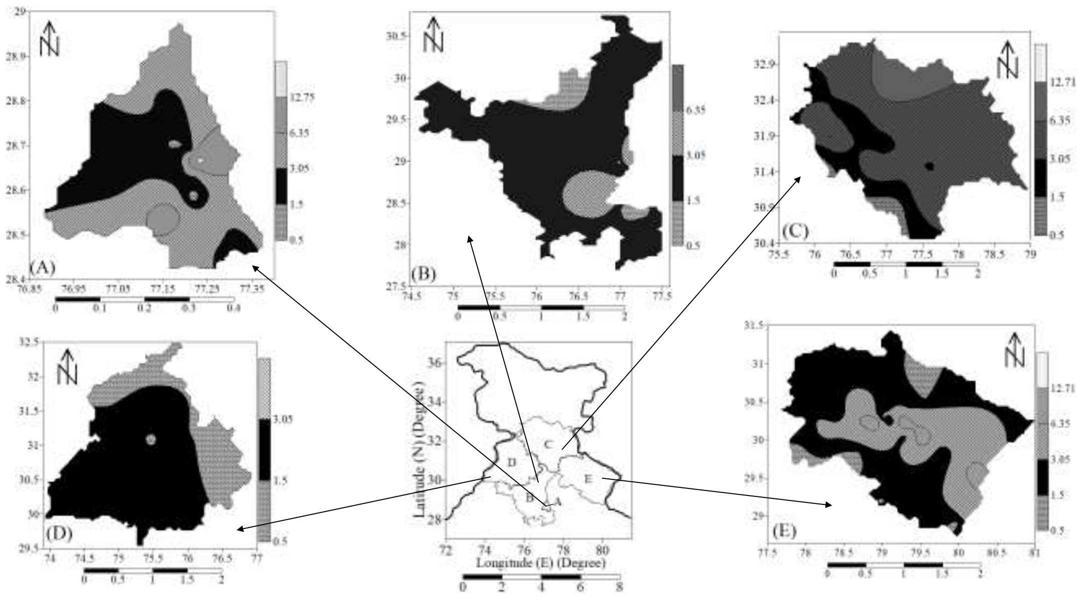

Figure 9. Spatial distribution of estimated f_{peak} for: (A) Delhi, (B) Haryana, (C) Himachal Pradesh, (D) Punjab and (E) Uttarakhand

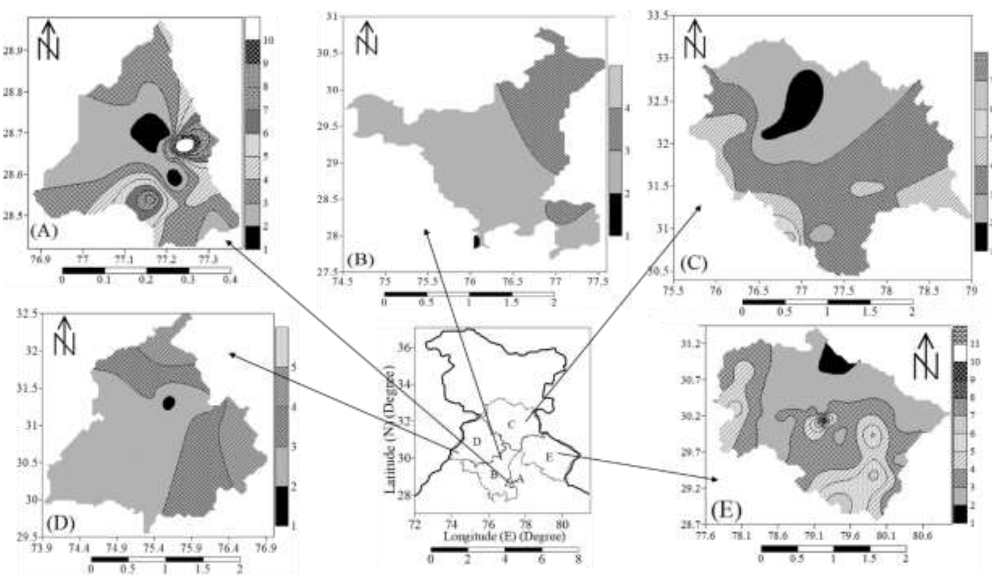

Figure 10: Spatial distribution of estimated A_{peak} for: (A) Delhi, (B) Haryana, (C) Himachal Pradesh, (D) Punjab and (E) Uttarakhand

Nat. Hazards Earth Syst. Sci. Discuss., https://doi.org/10.5194/nhess-2018-148
Manuscript under review for journal Nat. Hazards Earth Syst. Sci.
Discussion started: 10 July 2018

Natural Hazards and Earth System Sciences
Open Access
Discussions

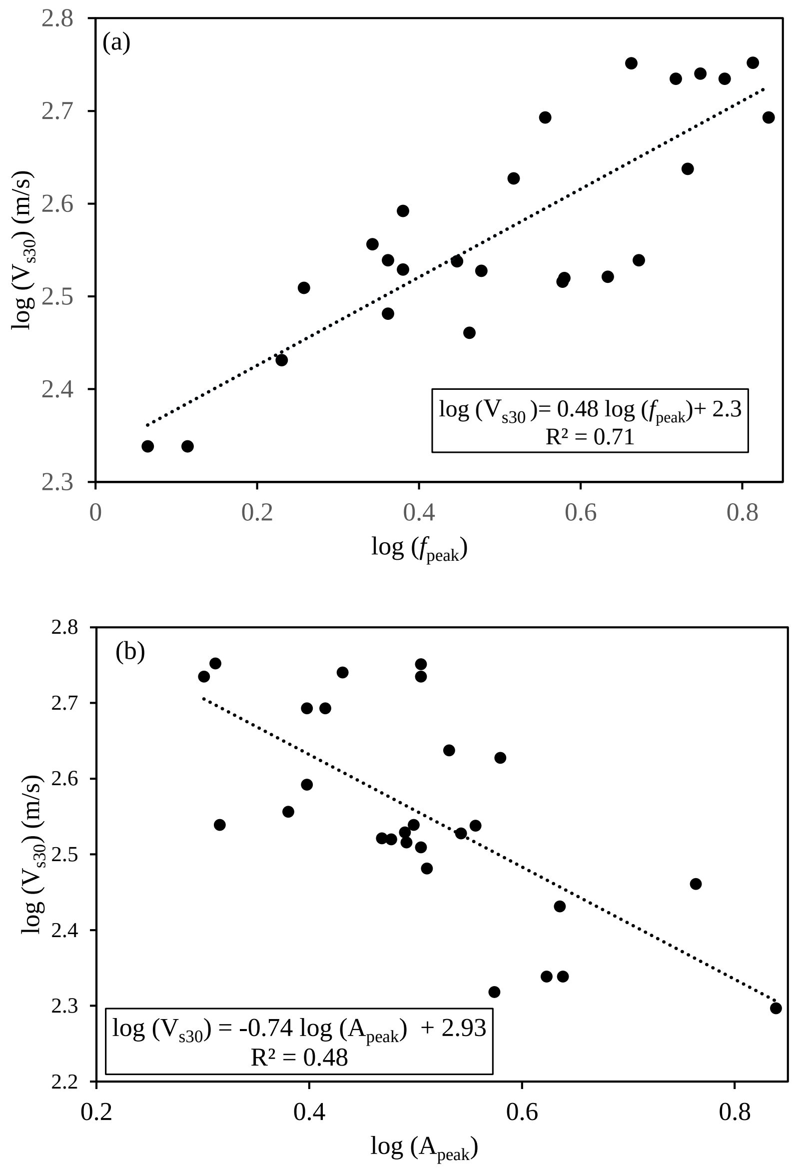

Figure 11: V_{s30} as a function of f_{peak} (a) and A_{peak} (b) of GINV method for recording stations at Delhi and Tarai region of Uttarakhand.

Nat. Hazards Earth Syst. Sci. Discuss., https://doi.org/10.5194/nhess-2018-148
Manuscript under review for journal Nat. Hazards Earth Syst. Sci.
Discussion started: 10 July 2018

TABLES

Table 1: Detail of strong motion recording stations.

Si. no	Station Code	Lat.(°) (N)	Lon. (°) (E)	GINV		HVSR		R* or S#
				f_{peak}	A_{peak}	f_{peak}	A_{peak}	
-1	-2	-3	-4	-5	-6	-7	-8	-9
	Himachal Pradesh							
1	AMB	31.7	76.1	1.7	4.3	1.2	9.3	S
2	BHA	31.6	77.9	4.5	4.0	4.1	4.4	S
3	CHM	30.4	79.3	1.4	5.4	1.5	7.5	S
4	DEH	31.9	76.2	6.8	3.5	10	5.4	R
5	DHH	32.2	76.3	2.7	4.5	2.7	4.9	S
6	HAM	31.7	76.5	2.9	3.3	3.1	6.6	S
7	JUB	31.1	77.7	5.8	3.3	5.6	4.9	S
8	KLG	32.6	77.0	8.0	1.8	8.3	2.2	R
9	KUL	32.0	77.1	3.3	2.3	3.1	3.0	S
10	MAN	31.7	76.9	2.5	3.4	2.3	5.3	S
11	RAM	31.4	77.6	2.8	4.2	2.7	5.6	S
12	SAL	32.7	76.1	2.7	3.0	2.7	5.8	S
13	SND	31.5	76.9	5.0	3.5	5.0	4.2	S
14	SOL	30.9	77.1	0.5	2.6	0.6	4.6	S
15	UNA	31.5	76.3	1.5	3.9	1.8	6.0	S
16	KJK	30.9	76.9	0.7	6.4	0.4	12.0	S
17	PLM	32.1	76.5	1.7	1.8	1.6	2.2	S
	Punjab							
1	ANS	31.2	76.5	0.9	4.9	0.9	17.0	S
2	ASR	31.6	74.9	1.0	2.9	1.0	8.0	S
3	GSK	31.2	76.1	0.8	2.3	0.8	3.8	S
4	JAL	31.3	75.6	2.9	1.5	2.9	1.7	S
5	KAT	31.4	75.4	2.0	3.1	3.0	3.4	S
6	MOG	30.8	75.2	2.2	2.3	2.2	3.9	S
7	MUK	31.9	75.6	1.4	4.7	1.4	15.9	S
8	NAW	31.1	76.1	1.4	3.6	1.4	3.5	S
9	NKD	31.1	75.5	1.2	2.2	1.3	3.4	S
10	PHG	31.2	75.8	2.7	2.7	2.7	5.2	S
11	TAR	31.4	74.9	2.6	2.7	2.7	4.6	S
	Delhi							
1	ARI	26.1	77.5	2.7	3.2	2.5	7.0	S
2	IGN	28.5	77.2	3.6	2.6	4.5	3.9	S
3	JNU	28.5	77.2	9.0	2.1	8.7	3.5	R
4	DJB	28.7	77.2	2.2	3.2	10	4.5	S
5	NDI	28.7	77.2	6.8	2.5	7.2	3.7	R
6	IMD	28.7	77.2	6.0	2.0	6.3	2.9	S
7	NTPC	28.5	77.3	2.8	3.6	2.8	5.4	S
8	ANC	28.5	77.3	4.6	3.2	4.5	4.5	S
9	JAMI	28.6	77.3	4.7	3.2	4.5	7.3	S

Si. no	Station Code	Lat.(°) (N)	Lon. (°) (E)	GINV		HVSR		R* or S#
				f_{peak}	A_{peak}	f_{peak}	A_{peak}	
-1	-2	-3	-4	-5	-6	-7	-8	-9
	Uttarakhand							
1	ALM	29.6	79.7	2.1	3.0	2.8	4.4	S
2	BAG	29.8	79.8	1.5	4.7	1.5	5.2	S
3	BAR	30.8	78.2	3.0	4.5	2.8	7.0	S
4	CHM	32.6	76.1	3.6	2.4	2.0	2.9	S
5	CHP	29.3	80.1	5.4	5.2	5.6	6.5	S
6	CKR	30.7	77.9	2.1	3.8	2.0	4.5	S
7	CMB B	30.0	79.5	8.3	2.7	8.3	6.3	R
8	DHA	29.8	80.5	3.1	3.3	2.7	5.5	S
9	DNL	30.4	78.2	2.8	3.3	2.0	7.1	S
10	DUN	30.3	78.0	2.9	5.8	3.1	7.1	S
11	GAR	30.1	79.3	2.4	3.4	2.3	4.5	S
12	GHA	30.4	78.7	5.2	2.3	4.5	5.5	S
13	GLTR	30.3	79.1	2.9	3.5	2.8	6.1	S
14	JSH	30.5	79.6	1.4	2.2	1.5	3.0	S
15	KAP	29.9	79.9	3.7	6.4	3.3	9.2	S
16	KHA	28.9	80.0	1.3	4.2	2.0	8.0	S
17	KKHR	30.2	78.9	9.5	3.5	9.5	9.3	R
18	KOT	29.7	78.5	0.7	2.4	0.7	3.3	S
19	KSK	29.2	79.0	3.1	3.8	3.2	9.9	S
20	KSL	30.9	77.0	3.0	3.9	2.1	19.4	S
21	LANG	30.3	79.3	7.7	2.8	7.9	5.7	R
22	LAN	29.8	78.7	1.4	2.8	1.4	6.1	S
23	MUN	30.1	80.2	4.3	2.8	7.0	3.6	S
24	PAU	30.2	78.8	5.9	2.1	3.1	3.7	S
25	PTH	29.6	80.2	8.0	2.7	4.6	3.1	R
26	PTI	29.4	79.9	4.0	6.6	3.6	8.0	S
27	RIS	30.1	78.3	3.8	3.0	3.4	6.4	S
28	ROO	29.9	77.9	1.2	4.4	1.3	5.2	S
29	RUD	30.3	79.0	1.3	2.8	1.5	4.2	S
30	SMLI	30.2	79.3	9.1	3.3	8.7	6.1	R
31	TAN	29.1	80.1	5.4	3.4	5.0	6.3	S
32	THE	30.4	78.4	1.6	2.8	1.5	3.6	S
33	UDH	29.0	79.4	2.7	6.9	2.2	10.1	S
34	UTK	30.7	78.4	2.4	2.9	2.3	4.4	S
35	VIK	30.5	77.8	2.3	3.8	2.3	10.4	S
36	GDRI	30.2	78.7	6.0	3.4	5.1	4.8	S
37	TLWR	30.3	79.0	1.1	2.1	1.0	4.6	S
38	UKMB	30.3	79.1	1.0	2.9	1.4	10.0	S
39	ADIB	30.2	79.2	6.4	12.7	6.3	17.8	R

Nat. Hazards Earth Syst. Sci. Discuss., https://doi.org/10.5194/nhess-2018-148
Manuscript under review for journal Nat. Hazards Earth Syst. Sci.
Discussion started: 10 July 2018

Natural Hazards and Earth System Sciences
Open Access
Discussions

10	LDR	28.6	77.2	0.7	4.3	0.9	7.0	S
11	VCD	28.6	77.2	4.6	2.7	4.6	3.6	S
12	IIT	28.6	77.3	4.3	2.9	4.5	4.3	S
13	NSIT	28.6	77.0	2.4	2.5	2.3	3.9	S
14	RGD	28.7	77.1	2.3	2.1	2.9	3.8	S
15	GGI	28.7	77.2	15	5.3	15	8.4	R
16	DLU	28.7	77.2	1.8	3.2	1.9	3.7	S
17	DCE	28.8	77.1	3.8	3.1	4.7	4.2	S
18	IGI	28.6	77.1	2.2	2.4	2.2	3.8	S
19	ZAKI	28.6	77.2	3.9	3.5	3.9	8.4	S
20	ALIP	28.8	77.1	2.3	3.2	2.5	6.9	S
21	ROI	28.6	77.2	1.4	3.1	2.0	4.6	S
40	NUTY	30.2	79.2	4.8	2.4	4.7	4.3	S
41	KHIB	30.2	78.8	7.7	3.3	8.0	8.7	R
42	STRK	30.3	79.0	4.7	2.8	4.7	5.8	S
43	NANP	30.3	79.3	3.9	3.5	3.8	9.1	S
	Haryana							
1	PAL	28.1	77.3	2.8	2.7	2.9	3.4	S
2	JAFR	28.6	76.9	6.0	2.0	7.1	2.6	S
3	GUR	28.4	77.0	1.0	4.1	1.0	5.2	S
4	REW	28.2	76.6	2.5	2.1	2.5	3.7	S
5	SON	29.0	77.0	1.0	3.5	2.8	4.0	S
6	ROH	28.6	77.2	1.4	3.1	2.0	4.6	S
7	CRRI	29.0	77.1	4.3	3.5	4.4	9.3	S
8	BAL	28.3	77.3	1.5	3.0	1.4	5.8	S
9	KAI	29.8	76.4	1.2	3.0	1.2	6.5	S

R* Rock site
S# Soil site

Table 2: Details of earthquakes considered for estimation of site parameters in this work.

Event No.	dd/mm/yyyy	Lat.	Long.	Depth	Magnitude	Event No.	dd/mm/yyyy	Lat.	Long.	Depth	Magnitude
-1	-6	-2	-3	-4	-5	-1	-6	-2	-3	-4	-5
1	14-12-2005	30.9	79.3	25.7	5.2	44	24-09-2011	30.9	78.3	10.0	3.0
2	07-05-2006	28.7	76.6	20.2	4.1	45	26-10-2011	31.5	76.8	5.0	3.5
3	29-11-2006	27.6	76.7	13.0	3.9	46	16-01-2012	29.7	78.9	10.0	3.6
4	10-12-2006	31.5	76.7	33.0	3.5	47	12-03-2012	28.9	77.3	5.0	3.5
5	22-07-2007	29.9	77.9	33.0	5.0	48	26-02-2012	29.6	80.8	10.0	4.3
6	25-11-2007	28.6	77.0	20.3	4.3	49	27-03-2012	26.1	87.8	12.0	3.5
7	04-10-2007	32.5	76.0	10.0	3.8	50	05-03-2012	28.7	76.6	14.0	4.9
8	18-10-2007	28.3	77.6	5.6	3.6	51	28-07-2012	29.7	80.7	10.0	4.5
9	19-08-2008	30.1	80.1	15.0	4.3	52	23-08-2012	28.4	82.7	5.0	5.0
10	19-10-2008	29.1	76.9	7.0	3.2	53	02-10-2012	32.4	76.4	10.0	4.9
11	21-10-2008	31.5	77.3	10.0	4.5	54	03-10-2012	32.4	76.3	10.0	3.6
12	31-01-2009	32.5	75.9	10.0	3.7	55	06-11-2012	32.3	76.2	5.0	4.1
13	09-01-2009	31.7	78.3	16.0	3.8	56	11-11-2012	29.3	80.1	5.0	5.0
14	25-02-2009	30.6	79.3	10.0	3.7	57	15-11-2012	30.2	80.1	5.0	3.0
15	18-03-2009	30.9	78.2	10.0	3.3	58	27-11-2012	30.9	78.4	12.0	4.8
16	04-09-2008	30.1	80.4	10.0	5.1	59	19-12-2012	28.6	76.8	10.0	2.9
17	01-05-2009	29.9	80.1	10.0	4.6	60	02-01-2013	29.4	81.1	10.0	4.8

Nat. Hazards Earth Syst. Sci. Discuss., https://doi.org/10.5194/nhess-2018-148
Manuscript under review for journal Nat. Hazards Earth Syst. Sci.
Discussion started: 10 July 2018

Natural Hazards and Earth System Sciences
Open Access
EGU
Discussions

18	15-05-2009	30.5	79.3	15.0	4.1
19	17-07-2009	32.3	76.1	39.3	3.7
20	27-08-2009	30.0	80.0	14.0	3.9
21	21-09-2009	30.9	79.1	13.0	4.7
22	03-10-2009	30.0	79.9	15.0	4.3
23	06-12-2009	35.8	77.3	60.0	5.3
24	11-01-2010	29.7	80.0	15.0	3.9
25	22-02-2010	30.0	80.1	2.0	4.7
26	24-02-2010	28.6	76.9	17.0	2.5
27	14-03-2010	31.7	76.1	29.0	4.6
28	03-05-2010	30.4	78.4	8.0	3.5
29	28-05-2010	31.2	77.9	43.0	4.8
30	31-05-2010	30.0	79.8	10.0	3.6
31	06-07-2010	29.8	80.4	10.0	5.1
32	10-07-2010	29.9	79.6	10.0	4.1
33	26-01-2011	29.0	77.2	10.0	3.2
34	14-03-2011	30.5	79.1	8.0	3.3
35	18-02-2011	28.6	77.3	5.0	2.3
36	09-02-2011	30.9	78.2	10.0	5.0
37	04-04-2011	29.6	80.8	10.0	5.7
38	15-06-2011	30.6	80.1	10.0	3.6
39	20-06-2011	30.5	79.4	12.0	4.6
40	23-06-2011	30.0	80.5	5.0	3.2
41	28-07-2011	33.3	76.0	21.0	4.4
42	07-09-2011	28.6	77.0	8.0	4.2
43	21-09-2011	30.9	78.3	10.0	3.1
61	09-01-2013	29.8	81.7	5.0	5.0
62	10-01-2013	30.1	80.4	5.0	3.2
63	29-01-2013	30.0	81.6	7.0	4.0
64	11-02-2013	31.0	78.4	5.0	4.3
65	17-02-2013	30.9	78.4	10.0	3.2
66	01-05-2013	33.1	75.8	15.0	5.8
67	05-09-2013	30.9	78.5	11.0	3.5
68	11-11-2013	28.5	77.2	10.0	3.1
69	11-11-2013	28.4	77.2	11.0	2.8
70	11-11-2013	28.4	77.2	12.0	2.5
71	11-11-2013	28.4	77.2	13.0	3.1
72	16-04-2013	28.0	62.1	16.0	7.8
73	04-06-2013	32.7	76.7	18.0	4.8
74	05-06-2013	32.8	76.3	10.0	4.5
75	09-07-2013	32.9	78.4	10.0	5.1
76	13-07-2013	32.2	76.3	10.0	10.0
77	15-07-2013	32.6	76.7	30.0	4.4
78	02-08-2013	33.5	75.5	20.0	5.4
79	29-08-2013	31.4	76.1	10.0	4.7
80	20-10-2013	35.8	77.5	80.0	5.5
81	25-12-2013	31.2	78.3	10.0	4.0
82	17-06-2014	32.2	76.1	10.0	4.1
83	21-08-2014	32.3	76.5	10.0	5.0
84	29-11-2015	30.6	79.6	15.0	4.0
85	25-09-2016	30.0	79.5	11.0	3.7
86	01-12-2016	30.6	79.6	19.0	4.0

Table 3: List of Earthquakes and the corresponding stations considered for the estimation of path parameter.

Earthquake Event	Stations
25-11- 2007	HGR, NDI, CRRI, PAL, REW, NDI , CRRI, LDR, JAFR, IIT
19-08-2008	CHP, PTH, KAP, MUN

Nat. Hazards Earth Syst. Sci. Discuss., https://doi.org/10.5194/nhess-2018-148
Manuscript under review for journal Nat. Hazards Earth Syst. Sci.
Discussion started: 10 July 2018

Natural Hazards and Earth System Sciences
Discussions

04-09- 2008	MUN, CHP, PTH, DHA , KAP, GHA, JSH
01-05-2009	MUN, BAG, KAP, GAR, CHM
17-07-2009	DHA, KLG
27-08-2009	KAP, BAG, MUN
03-08-2009	KAP, CHP, BAG
11-01-2010	PTH, CHP, DHA
22-02-2010	KAP, BAG, DHA, ROO, UDH
24-02-2010	RGD, IGN, ROH, DJB, CHP, ANC, JAMI, GGI, DLU, DCE
14-03-2010	DEH, JUB, SND, BHA, HAM, GAR, JAL, KAP, AMB, ROO
03-04-2010	THE, BAR, DNL, ROO
28-05-2010	JUB, BAR, ROO, UNA
06-06-2010	MUN, CHP
10-07-2010	BAG, KAP, GAR, ROO
18-02-2011	DJB, ANC
09-02-2011	UTK, SND, KUL, CKR
04-04-2011	JSH, CHP, PTI, PTH, ALM, DDH, BAG, DHA, GAR, MUN, RUD, THE, CHM, BAR, SND, KOT, DNL, LDR, ROO, TAN, KHA, UDH, KSH, DUD
12-03-2012	GGI, ANC, DLU, DCE
27-03-2012	ARI, ANC
05-03-2012	JAFR, JNU, DJB, IMD, PLW, GUR, NOI, NTPC, ANC, IIT, NSIT, ZAKI, ROO, RGD, GGI, DLU, DCE, ALIP, SON, BAR, KAI, NKD,
02-10-2012	CHA, RAM
11-11-2012	CHA, CHP, PTH
27-11-2012	UTK, THE, DNL, CKR
02-01-2013	CHP, PTI, PTH
09-01-2013	CHP, PTI, PTH, TAN
11-02-2013	UTK, ROO
11-11-2013 (19:11:18)	NTPC, IGN, JNU, DJB, IMD, VCD, IGI, RGD, GGI, DLU, DCE, ALIP
11-11-2013 (22,10,42)	IGN, JNU, DJB, VCD, RGD, DCE, ALIP
11-11-2013 (20:11:30)	IGN, JNU, DJB, VCD, RGD, GGI, DLU, DCE
29-08- 2013	GSK, RAM, ROO, NKD, ANS, KAT
25-09-2016	UKMB, CMBB, GDRI, DURD

Table 4: Resulting parameters of eq. 7.

f (Hz)	m	$Q_0 = {(\pi f)}/{(\beta m)}$
(1)	(2)	(3)
0.50	0.0095	51.65
1.00	0.0101	97.15
1.75	0.0115	149.32
2.50	0.0096	255.53
3.12	0.0089	344.54
3.57	0.0093	376.67
4.50	0.0098	450.57
5.00	0.0074	663.01
5.50	0.0089	606.39
6.25	0.0084	730.09
7.14	0.011	636.92
8.00	0.013	603.84
10.00	0.0172	570.49
11.76	0.0124	930.60
12.50	0.0102	1202.51
13.33	0.0098	1334.70

14.28	0.0115	1218.46
15.00	0.0108	1362.85

Table 5: $f_{peak,}$ A_{peak} and V_{s30} values for 27 stations located in Terai region of Uttarakhand and Delhi region.

	GINV		
Station Code	$f_{peak,}$(Hz)	$A_{peak,}$	V_{s30} (m/s)
IGN	3.6	2.6	493*
JNU	6.5	2.05	565*
DJB	5.22	3.2	543*
NDI	6.8	2.5	493*
IMD	6	2	543*
NTPC	2.8	3.6	345*
ANC	4.6	3.2	564*
JAMI	4.7	3.15	346*
LDR	0.7	4.32	270*
VCD	5.6	2.7	550*
IIT	4.3	2.94	332*
NSIT	2.4	2.5	391*
RGD	2.3	2.07	346*
DLU	1.81	3.2	323*
DCE	3.78	3.1	328*
IGI	2.2	2.4	360*
ZAKI	3	3.49	337*
ROI	2.3	3.24	303*
ALIP	1.4	3.09	338*
DUN	2.9	5.8	289**
KHA	1.3	4.2	218**
KSK	3.13	3.75	208**
RIS	3.8	3	331**
ROO	1.16	4.35	218**
TAN	5.4	3.4	434**
UDH	2.74	6.9	198**
VIK	2.29	3.8	424**

**Pandey et al., 2016a; * Pandey et al., 2016b

Nat. Hazards Earth Syst. Sci. Discuss., https://doi.org/10.5194/nhess-2018-148
Manuscript under review for journal Nat. Hazards Earth Syst. Sci.
Discussion started: 10 July 2018

Natural Hazards and Earth System Sciences
Open Access
Discussions

List of Figures

List of Tables